ADSORPTION OF WATER AND CARBON MONOXIDE ON $Cu_2O(111)$ SINGLE CRYSTAL SURFACES

by

Anne-Claire Christiaen

Thesis submitted to the faculty of the

Virginia Polytechnic Institute and State University

in partial fulfillment of the requirements for the degree of

Master of Science

in

Chemical Engineering

APPROVED:

David F. Cox, Chairman

Eva Marand

Ted Oyama

August, 1994

Blacksburg, Virginia

ADSORPTION OF WATER AND CARBON MONOXIDE ON $Cu_2O(111)$ SINGLE CRYSTAL SURFACES

by

Anne-Claire Christiaen
Committee Chairman: David F. Cox
Chemical Engineering

(ABSTRACT)

Water and CO adsorptions were studied over the stoichiometric and the oxygen-deficient $Cu_2O(111)$ surfaces, using thermal desorption spectroscopy (TDS), ultraviolet photoelectron spectroscopy (UPS), and X-ray photoelectron spectroscopy (XPS). Water is the only desorbing species detected in TDS and the extent of dissociation is unaffected by the surface condition: $\simeq$ 0.25 monolayers of water dissociate on $Cu_2O(111)$ regardless of surface condition. The local defect environment around oxygen vacancies does not play a significant role in the activity of the $Cu_2O(111)$ surface for the dissociation of water. CO is found to bind molecularly to the surface through the carbon atom and with a heat of adsorption of 22 kcal/mol, higher value than that of CO on $Cu_2O(100)$ (16.7 kcal/mol). This suggests that the local geometry of adsorption sites may play an important role in the way CO binds to Cu_2O surfaces. Electronic changes upon CO adsorption and the higher heat of adsorption indicate an increased σ-donor character for CO, with some π-backbonding interactions. The local defect environment around oxygen vacancies does not appear to affect CO adsorption on $Cu_2O(111)$ surfaces.

ACKNOWLEDGEMENTS

I would like to thank my advisor, David F. Cox, for his support and guidance throughout my graduate studies at Virginia Tech. I am particularly thankful for the confidence he had in me, for his positive attitude in research, and for his professionalism in general.

I would like to thank the members of my committee for their time and effort as well as D.O.E. for financial support of my work.

I would also like to thank J. R. Mahan for the efforts he makes to offer graduate programs at Virginia Tech to half a dozen of French students every year. It is a wonderful experience for us made possible by him and all the personnel at the Université de Technologie de Compiègne (France).

Also, I would like to thank the French connection, Anne Vilette, Benoit Girardin and Eric Toffin for being a real family for me and without whom I would not enjoy life here, as well as my new "brother", Steve York.

Finally, I would like to thank my parents for the love and support they gave me and for being there when I need them. This thesis is dedicated to them.

TABLE OF CONTENTS

LIST OF FIGURES

LIST OF FIGURES

CHAPTER 1

Introduction

1.1 Background

The chemistry and physics of solid surfaces and interfaces play a vital role in many technologically important processes ranging from catalysis and corrosion to the operation of microelectronics devices. Surfaces are of great interest because they represent a rather special kind of defects in the solid state. Much of our understanding of solids is based on the fact that they are perfectly periodic in three dimensions. The introduction of a surface can lead to structural changes as well as to the introduction of localized electronic and vibrational states. Perhaps, the most widely quoted motivation for modern surface studies is the goal of understanding heterogeneous catalysis, among many other goal such as corrosion or fabrication of semiconductor devices. The greatly increased rates of certain chemical reactions which occur in the presence of solid catalysis must result from the modification of at least one of the constituent chemicals when adsorbed on the solid surface and its enhanced ability to interact with the other constituents in this state. One

would therefore like to understand what these modifications are, which type of sites are active on the catalyst surface and how these processes depend on the catalyst material.

Initial demonstrations of the photocatalytic properties of titanium oxides in aqueous media, presented in the seventies, have inspired work on well-characterized single-crystal oxides. These model studies, even if they may be far removed from applied catalytic problems to be of real value, help understanding many catalytic processes. Though they have been considered much less often than metals, metal oxides appear to offer some of the best opportunities for developing structure-reactivity relationships. As an example, reactions of carboxylic acids on different oxide single-crystal surfaces illustrates the roles of surface coordinative unsaturation, oxidation state, and redox properties in determining the surface reactivity of metal oxides.

Numerous studies indicate the important role of surface lattice oxygen in a reaction pathway. The degree of surface oxidation and the presence of reduced surface sites has been shown to influence both the selectivity and activity of oxide catalysts. Due to structural sensitivity which oxide catalysts can exhibit, the details of the local structure and electronic properties of defects such as oxygen vacancies can be quite important.

Surface properties of the oxygen/copper system have been investigated extensively for over twenty-five years in an effort to understand the structure and electronic properties of both adsorbed and incorporated oxygen. Recently, there has been a renewed interest in the

electronic properties of copper oxides because of the advances in high-Tc copper oxide superconductors. In heterogeneous catalysis, Cu_2O is the only reported single component oxide to catalyze, as an example, propene partial oxidation to acrolein as part of allylic oxidation reactions of olefins. Also, mechanistic information obtained over Cu_2O may be applicable to more complex mixed oxide systems.

Previous characterization work done on $Cu_2O(111)$ surfaces [18] has shown that the surface may be manipulated to introduce oxygen vacancies. This allows a determination of (1) the importance of surface cation coordination and (2) the adsorption sites for various reactions, such as the partial oxidation of propene to acrolein over Cu_2O single-crystal surfaces. The adsorption of CO and water on various surfaces have been subject to extensive work in the past years. CO and H_2O are two relatively simple molecules observed in many catalytic reactions. The focus of this thesis is on the interaction of water and CO with two types of $Cu_2O(111)$ surfaces, one being nearly stoichiometric and the other being oxygen-deficient, in order to characterize the effect of oxygen vacancies.

Water adsorption on surfaces, which shows an extensive variety of applications, is very important in heterogeneous catalysis. Traces of water can greatly change the selectivity of a reaction, as in the catalytic hydrogenation of benzene over ruthenium metal. Water molecules are known to adsorb molecularly and dissociatively. Dissociative adsorption of water is often observed to be enhanced by local defects (oxygen vacancies). The study of water adsorption on $Cu_2O(111)$ surfaces in given

in Chapter 2.

There has been much discussion in the literature concerning the nature of active sites, the intermediates involved and the mechanism of methanol synthesis from CO and H_2. Copper species in Cu/ZnO methanol synthesis catalysts have been observed to constitute active centers for the high activity of the Cu/ZnO catalysts for methanol synthesis: it is thought that Cu^+ sites bind CO more strongly than either Cu metal or ZnO [45]. The study of CO adsorption on $Cu_2O(111)$ surfaces in given in Chapter 3.

1.2 Surfaces investigated

The two low-index surfaces investigated differ both in the availability of surface lattice oxygen and the Cu^+ coordination number. The ideal, stoichiometric $Cu_2O(111)$ surface is illustrated in figure 1.1(a). As with other cubic crystals, it possesses hexagonal symmetry with a (1x1) LEED periodicity. No single atomic layer parallel to the $Cu_2O(111)$ contains both copper cations and oxygen anions. The copper planes parallel to the (111) surface contain four Cu^+ cations per unit cell, leading to a 4+ charge. Each copper-containing plane is sandwiched between two oxygen-containing planes. Each of these planes has one anion per surface unit cell, and a 2- charge. Thus, a three-plane repeat unit figure 1.1 satisfies stoichiometry and charge neutrality. Since the termination for a

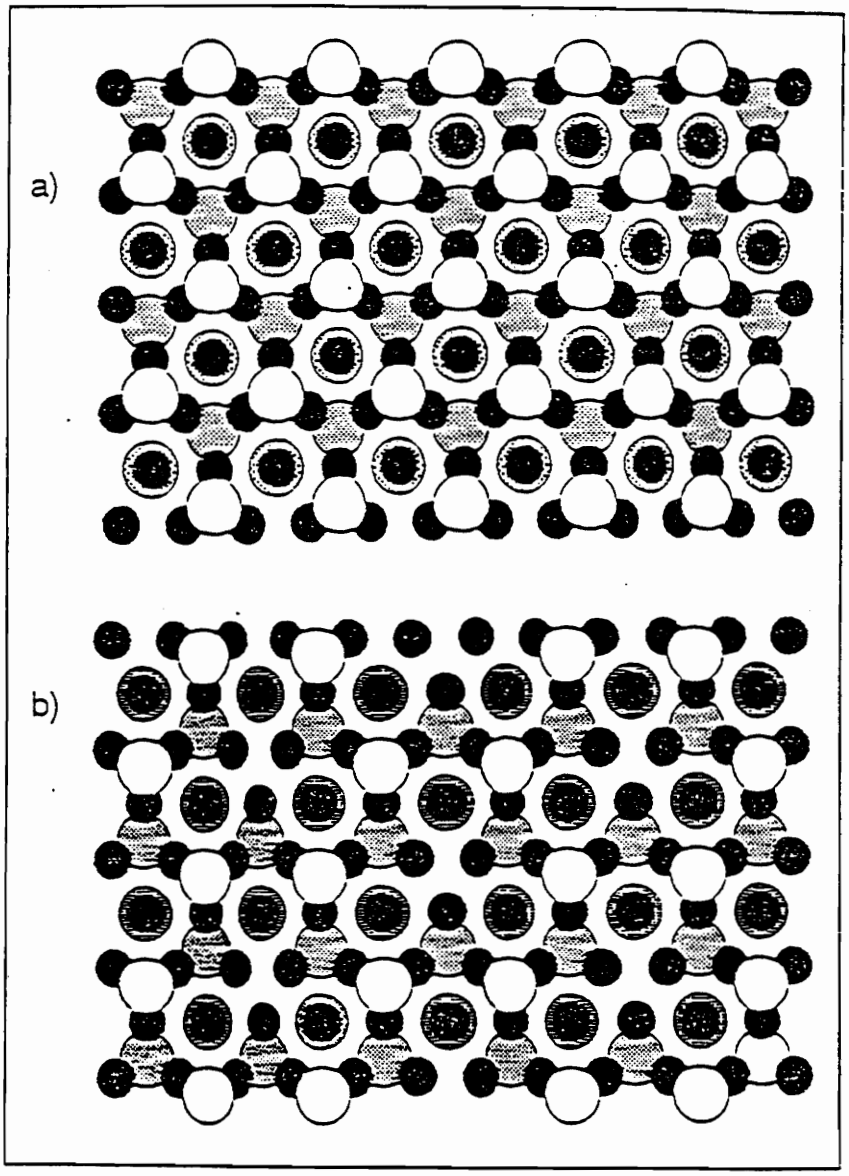

Figure 1.1 Ball model illustrations of (a) the ideal, stoichiometric, non-polar $Cu_2O(111)$ - (1x1) surface, and (b) the oxygen-deficient $Cu_2O(111)$ surface.
The small solid circles represent Cu^+ cations, while the large open circles represent O^{2-} anions. Drawing is based on the ionic radii of the ions, and assume no relaxation. Increased shading of the oxygen anions represents increasing distances away from the surface. For clarity, only the top four atomic layers are shown.

stoichiometric $Cu_2O(111)$ surface should be non polar based on surface-energy considerations [39], the outer atomic layer is composed of triply-coordinate oxygen anions (bulk lattice O^{2-} coordination = 4), the second atomic layer being composed of Cu^+ cations and the third atomic layer of oxygen anions. In the second atomic layer, copper cations can be either singly- or doubly-coordinate in the ratio of 1 to 4, respectively (bulk Cu^+ coordination = 2).

As shown before [1], this nearly stoichiometric surface can be prepared by ion bombardment (3 keV Ar-ion sputtering) followed by annealing to 1000 K for five minutes.

Formation of oxygen vacancies in the outer atomic layer has been observed previously following repeated exposures of the $Cu_2O(111)$ surface to reducing gases [6]. The (1x1) LEED periodicity is replaced by a $(\sqrt{3}x\sqrt{3})R30°$ LEED periodicity thought to be due to an ordered one third of a layer of oxygen vacancies [1]. Each oxygen vacancy gives rise to a threefold site of singly-coordinate Cu^+ cations in the second atomic layer. A ball model of the oxygen-deficient $Cu_2O(111)$-$(\sqrt{3}x\sqrt{3})R30°$ surface is illustrated in figure 1.1(b).

The surface was reduced by exposure to large doses ($\approx$ 450 L) of hydrogen with the surface maintained at approximately 450 to 500 K (water TDS studies have shown that atomic hydrogen extracts lattice oxygen to form water at about 500 K on $Cu_2O(100)$ [38]). Since H_2 does not dissociatively adsorb on the $Cu_2O(111)$ surface under UHV conditions [38], H_2 was dissociated using a hot platinum filament. Unlike previously [6], oxygen atoms were not removed in number sufficient to produce a

well-defined $Cu_2O(111)$ - $(\sqrt{3}x\sqrt{3})R30°$ periodicity LEED pattern [6]. The number of oxygen vacancies was estimated from the relative integrated areas of the TDS features obtained for 0.06 L of propene (see below) and compared to what was obtained for the well-defined $(\sqrt{3}x\sqrt{3})R30°$ surface. The oxygen vacancies were found to represent about one sixth of a layer. Also, oxygen vacancies appeared to be sensitive to the annealing temperature: annealing to 1000 K reordered the surface back to the (1x1) periodicity LEED pattern. This observation implies that mobile lattice oxygen diffuses from the bulk to the surface at higher temperatures, as reported previously for $Cu_2O(100)$ [1]. Thus, the oxygen deficient surface was only annealed to about 850 K. Nevertheless, after many repeated exposures were made, the (1x1) pattern could not be regained simply by annealing to 1000 K. Extended ion bombardment ($\approx$ 12 hours) was required to restore the surface to its original condition, such that annealing at 1000 K would again result in a (1x1) LEED pattern. Propene (0.06 L dose) was used as a sensitive probe of lattice oxygen vacancies on the $Cu_2O(111)$ surface. Indeed, previous studies of propene adsorption on $Cu_2O(111)$ using thermal desorption and photoemission [6] demonstrated that propene adsorption is structure-sensitive on Cu_2O single-crystal surfaces. In TDS, a distinct change of the number and temperatures of propene desorption features is observed as function of surface condition. When the surface progressively changes from a (1x1) to a $(\sqrt{3}x\sqrt{3})R30°$ LEED periodicity, a high-temperature (336 K) propene desorption feature increases whereas a lower-temperature feature (220 K), characteristic of the nearly stoichiometric (1x1) surface, decreases and shifts to higher

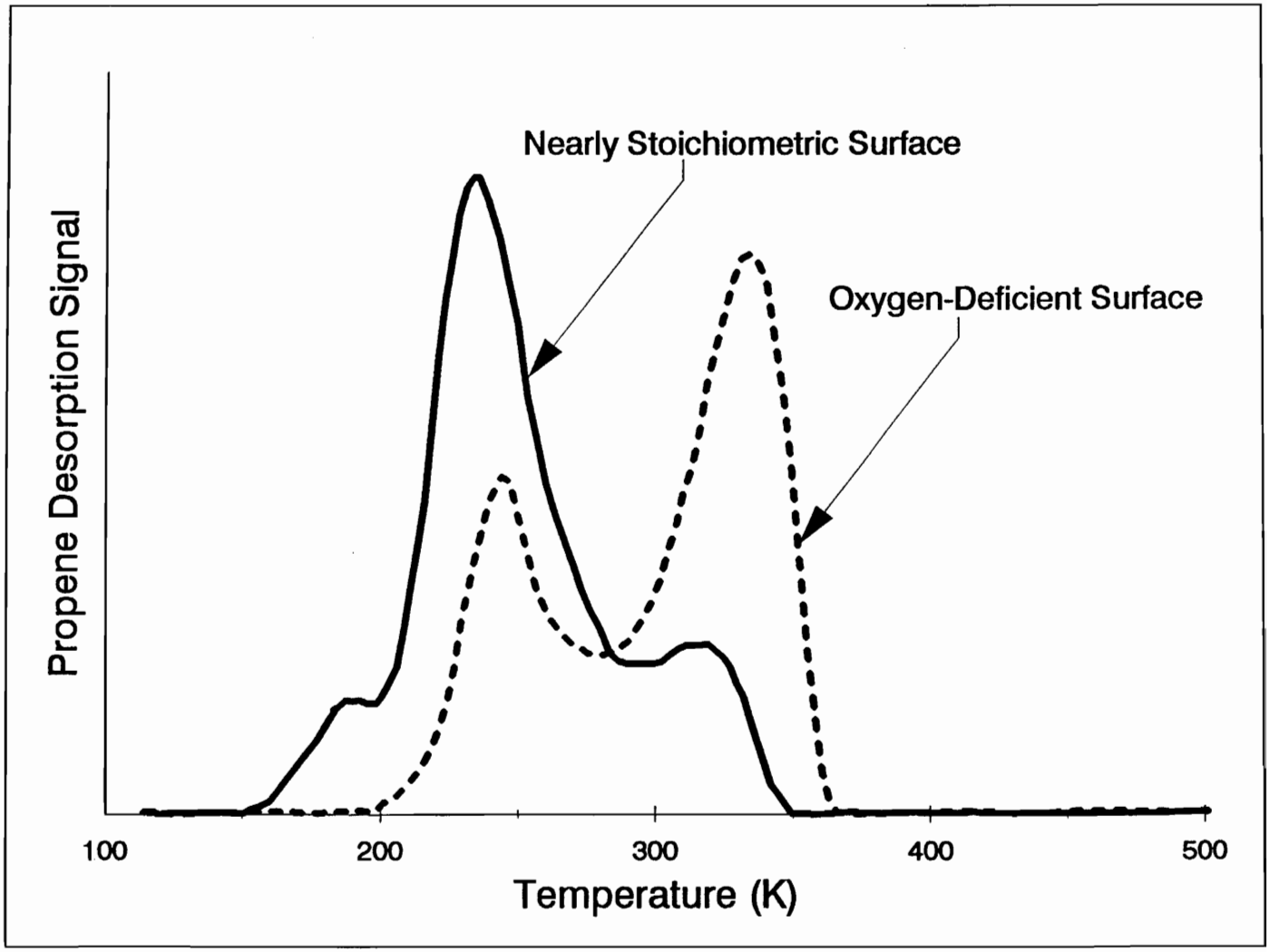

Figure 1.2 Thermal desorption spectra of 0.06 L propene doses from a nearly stoichiometric (solid line) and from an oxygen-deficient (dashed line) Cu_2O surfaces.

temperature (245 K) for the oxygen-deficient surface. These changes in the propene desorption features are illustrated on figure 1.2 for 0.06 L propene doses on both surfaces, the nearly stoichiometric surface (solid line) and the oxygen-deficient surface (dashed line), after reducing the stoichiometric surface with dissociated H_2. Thus, this 336 K feature is assigned to propene adsorption at or around the threefold Cu^+ sites associated with the 1/3 of lattice oxygen vacancies on the (111)-($\sqrt{3}$x$\sqrt{3}$)R30° surface.

The use of normal-emission XPS data for evaluating the oxygen-vacancies of the (111) surface was not possible. Indeed, the XPS Cu-to-O ratio for normal emission based on the mean-free-path dependence of the photoelectron (assuming no diffraction effects) varied within experimental error (0.05) for one third of oxygen vacancies on the surface [1].

1.3 Experiments

All experiments were conducted in a turbopumped dual-chamber stainless steel ultrahigh vacuum system. The analysis chamber (base pressure of 4 x 10^{-11} Torr) is equipped with a Leybold EA-11 hemispherical analyzer, a dual-anode Mg/Al x-ray source for x-ray photoelectron spectroscopy (XPS) and a differentially-pumped D.C.

discharge lamp for ultraviolet photoelectron spectroscopy (UPS). XPS spectra were collected using Mg/Kα radiation ($h\nu = 1253.6$ eV) exclusively, and run at a resolution of 1.03 eV FWHM on Ag $3d_{5/2}$. UPS data were collected with normal emission at an analyzer resolution (ΔE) of 0.15 eV, an incident angle of 55° with respect to the surface normal for normal emission and unpolarized He I ($h\nu = 21.2$ eV) and He II ($h\nu = 40.8$ eV) radiation.

The preparation chamber is equipped with a set of Vacuum Generator 3-grid reverse view LEED optics. A broad-beam ion gun was used in the preparation chamber for sample cleaning. An Inficon Quadrex 200 mass spectrometer monitored up to 6 masses simultaneously during thermal desorption spectroscopy (TDS).

Gas exposures up to 5 L (1 L $\equiv$ 1×10^{-6} Torr.s) were performed by backfilling the chamber through a variable leak valve. The values indicated for CO doses have not been corrected for ion gauge sensitivity: the real doses are within 5 % of the indicated values. Aldrich HPLC grade water was used following degassing by repeated freeze-pump-thaw cycles. Matheson Research grade CO (99.997%) was used as received. Matheson Polymer-grade propene (99.5%) containing 0.4 % propane as the major contaminant and Matheson Research-grade H_2 (99.9995%) were used as received.

For TDS experiments, a 2 K/s linear temperature ramp was used. This low heating rate (2 K/s) was used to minimize the possibility of thermal fracture of the ceramic Cu_2O sample. The mass spectrometer was equipped with a quartz skimmer to minimize the sample of desorption

products from the crystal hardware. Blank experiments on the clean surface showed that the amount of contribution from the crystal hardware and the background uptake were negligible. The background pressure between doses was kept under $2x10^{-10}$ Torr.

The crystal was grown by a float zone technique using an arc image furnace [33]. It was aligned using Laue back scattering, and mechanically polished to within $\pm 0.5°$ of the (111) surface in order to give an optically smooth surface. Sample dimensions were approximately 7 x 5 x 1 mm^3.

The oxygen-deficient surface was prepared by exposure to H_2 gas in the preparation chamber with a hot platinum filament located approximately 15 mm from the sample surface.

The sample cleanliness was monitored with XPS, and the average value for the sensitivity-corrected Cu-to-O ratio was about 1.75 [1].

The crystal used in this study is the same used previously [1] and the sample preparation and characteristics are those expected for a surface which has undergone many ion bombardments and annealing cycles.

The sample was clamped to a tantalum support with tantalum shims. The holder was connected to LN_2-cooled copper electrical feed-throughs in a sample rod manipulator by two 0.127 mm-thick strips of tantalum foils. The holder acted both as a stable mechanical support and an indirect heating and cooling source. A type-K thermocouple was bonded directly to the back of the Cu_2O crystal with Aremco #569 ceramic cement through a small hole in the tantalum holder, thus allowing a direct measure of the crystal temperature. The temperature could be

varied from 100 to 1000 K.

Cuprous oxide, Cu_2O, is a p-type semiconductor with the cuprite structure ($Pn3$). The sample used in this study had a bulk resistivity of about 10^3 Ω cm at room temperature. While the sample is conductive at room temperature, steady-state charging was observed during photoemission measurements near 100 K. To account for charging at low temperatures, all UPS binding energies are referenced to the valence-band maximum (VBM). A negative 5 V bias was applied to the sample to allow for an accurate measure of the total width of the photoelectron emission independent of analyzer work function. Because the extent of charging is temperature dependent, the sample temperature was maintained at about 140 K while UPS data were collected. Gas exposures were performed at the lowest temperature ($\approx$ 100 - 110 K) the sample could reach. Near 140 K, the variations in steady-state charging had no effect on the measured width of the photoelectron distribution. Likewise, no evidence for differential charging was observed. The photoemission peak shapes and FWHMs were the same as those collected at room temperature.

CHAPTER 2

Water Adsorption on $Cu_2O(111)$ Single Crystal Surfaces

2.1 Introduction

Water is one of the most studied adsorbates on well-defined metal **oxide** single-crystal surfaces. Water adsorption at surfaces shows an extensive variety of applications: in meteorology (investigation of the mechanism of ice or water nucleation at surfaces to understand cloud-seeding and precipitation [1]), in geology (investigation of the forces which produce particular arrangements of water molecules in ice to understand glacial history [2]), in electrochemistry (the formation of a layer of water molecules near a metal electrode surface plays a key role in electrochemical reactions [3]), in solar energy conversion processes (which splits the water molecules [4]), in physical chemistry (investigation of the structure of small H_2O clusters and nature of hydrogen bonding between water molecules [5]) or in heterogeneous catalysis. More specifically, numerous catalytic reactions, such as the Fischer-Tropsch synthesis of hydrocarbons, involve water as a reactant or a product. Also, water is

seen to be a desorption product during atomic hydrogen adsorption [6]. Water may also interfere and contaminate a surface during oxygen adsorption.

Water molecules have been seen to adsorb molecularly and dissociatively. On metals, water has been observed to dissociate and form OH and H [7], dissociate completely to O and H [8], or dissociate as O, H, and OH [9].

Powder surfaces of a large number of common oxides are easily hydroxylated [10]. However, well-ordered single-crystal surfaces have been found to be less reactive for H_2O dissociation [11,12,13,14]. The influence of surface imperfections or defects (e.g., oxygen vacancies as the most commonly accepted type of defects) and of non-lattice oxygen in catalyzing the dissociation of water has been demonstrated previously [10,15]. However, in a previous study of $Cu_2O(100)$ surfaces, defects were not found to affect water dissociation [16]. The focus here is on the well-defined single-crystal $Cu_2O(111)$ in order to try to answer to the following questions: (1) is the adsorption of water at 110 K molecular or dissociative, (2) what are the dissociation products and (3) the site requirements for dissociation? Do oxygen vacancies affect the water dissociation process since it is thought that an available lattice oxygen anion (O^{2-}) ties up H^+ as OH^-, while an available cation coordinates the conjugate base anion, OH^-? Is the dissociation of water on Cu_2O surfaces orientation (structure) sensitive?

2.2 Results

2.2.1 Thermal Desorption Spectroscopy

The adsorption of water was examined by TDS on the stoichiometric and oxygen-deficient surfaces described above. Both surfaces were exposed to water at 110 K and heated linearly at 2 K/s to 700 K. Only water was observed as a desorption product in TDS following water adsorption. H_2 or O_2 were not detected as desorption products. However the hydrogen background in the vacuum system was high enough that some H_2 desorption might have gone undetected. As shown below, the desorption behavior of H_2O is similar on both the stoichiometric and reduced surfaces.

2.2.1.1. Nearly stoichiometric surface

The coverage dependance of the H_2O desorption traces for the nearly stoichiometric surface at 100 K is illustrated in figure 2.1. The left panel shows the low coverage regime (doses less than 0.5 L) and the right panel shows the high coverage regime (doses up to 5 L). At the lowest dose investigated, 0.03 L, a H_2O feature was observed with a peak temperature, Tp, of 230 K along with a small, broad, higher-temperature feature centered at about 290 K. Larger doses result in additional features.

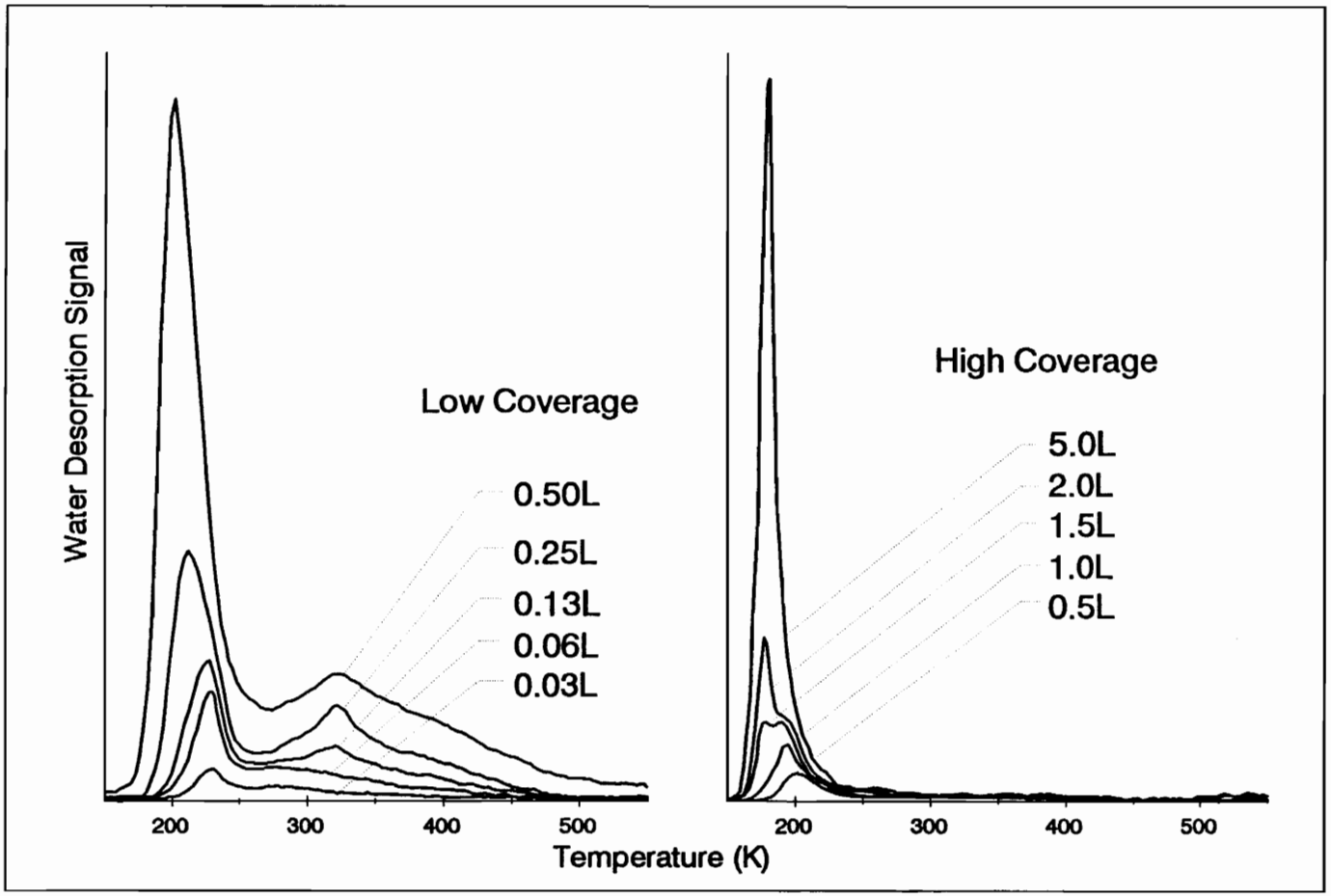

Figure 2.1 Thermal desorption traces for water following adsorption at 110 K on the nearly stoichiometric $Cu_2O(111)$ surface.

A clear maximum appears at about 322 K for doses of 0.13 L and greater, and this feature broadens to higher temperatures out to about 450 K. The lower temperature feature grows in as well with larger doses, and shifts from 230 K to 190 K with increasing coverage. For doses between 0.5 L and 1 L, this feature dominates the desorption traces, and the high temperature ($\simeq$ 322 K) feature makes only a small contribution to the overall water signal. For doses above 1 L, an additional feature appears at 177 K. This feature increases without saturation, thus providing clear evidence of multilayer desorption. The multilayer feature shifts to higher temperature with increasing coverage, 181 K for a 5 L dose, a characteristic of zero-order multilayer sublimation [10].

Our multilayer temperature is about 20 K higher than the temperature reported previously for multilayer ice on numerous metals [10], such as Pt, Pd, Ru, Rh or Ag [7,21,22,23,24]. We apparently get a small contribution to the thermocouple reading from the tantalum holder used. Assuming that this contribution stays constant over the temperature range studied, the error due to the temperature offset on the estimate for a first-order activation energy of desorption should not be greater than 1.3 kcal/mol.

It is noted that no desorption feature is clearly resolved in the high-temperature range (400 K - 500 K) as observed previously in the literature on other well-defined oxide surfaces [16,25,12]. Nevertheless, the feature near 320 K tends to broaden to about 450 K - 500 K. The primary contribution to this feature at 320 K appears to be first-order, identified by the nearly constant peak temperature with changing coverage

[26] for doses up to 0.5 L, and not second-order as expected for an elementary reaction such as OH disproportionation. Using the Redhead equation [26] and assuming a normal first-order pre-exponential of 10^{13} s^{-1} gives a first-order activation energy of 20.1 kcal/mol for the rate-limiting step of the 320 K desorption feature. However, the broadness of this feature suggests that there may be more than one contribution to the desorption signal above 320 K. Given the broadness of the high-temperature component of the signal, no clear assignment of a reaction order can be made except for the apparent first-order contribution at 320 K described above. Using the integrated area under the 190 K peak of the 1.5 L trace as being representative of a monolayer coverage, the desorption signal originating from the high-temperature feature is estimated to represent about 25 ± 5 % of a monolayer. As will be shown below (section 2.2.2), this part of the desorption signal representing about 25 ± 5 % of a monolayer is due to the recombination of dissociated water, while the feature with 190 K ≤ Tp ≤ 230 K is due to desorption of a molecular water surface species.

Assuming that the shift to lower temperatures with coverage for the 190 K ≤ Tp ≤ 230 K water desorption feature is due to the variations in the strength of the bond between the molecular water (vide infra) and the surface, we can assume first-order kinetics for the 190 K ≤ Tp ≤ 230 K feature. The Redhead equation [26] gives a range for the first-order activation energy of desorption of 11.6 - 14.2 kcal/mol for molecular water desorption assuming a normal first-order pre-exponential of 10^{13} s^{-1}.

2.2.1.2. Oxygen-deficient surface

The coverage dependance of the H_2O traces for the oxygen-deficient $Cu_2O(111)$ surface is illustrated in figure 2.2. Only the low-coverage dose range (up to 0.5 L) is represented, the high-coverage data showing the same trend as that observed for the high-coverage of H_2O on the nearly stoichiometric surface in figure 2.1. We clearly observed a high-temperature feature near 315 K for doses up to 0.5 L. As the coverage increases up to 1 L, a feature grows in at lower temperature and dominates the desorption traces. The peak temperature of this feature decreases with increasing coverage from 230 K for a 0.06 L to 196 K for 1 L. For larger doses, the multilayer temperature feature increases without saturation near 178 K. The main difference is seen for the lowest H_2O dose, 0.03 L. The feature observed on the nearly stoichiometric surface at 230 K does not appear. Instead, the broad peak near 290 K appeared near 274 K. These variations in the TDS traces for this low dose do not appear to be significant, since the accuracy of such low doses is limited by the slow pumping speed of water in the vacuum system.

Using the Redhead equation [26], the first-order activation energy for desorption associated with the 315 K feature is 19 kcal/mol, within 1 kcal/mol of the value for the nearly stoichiometric surface. The first-order energy for desorption associated with the feature near 196 K is determined to be in the range 12 - 14.2 kcal/mol for the limiting step of molecular water desorption.

The TDS results on $Cu_2O(111)$ surfaces demonstrate that water

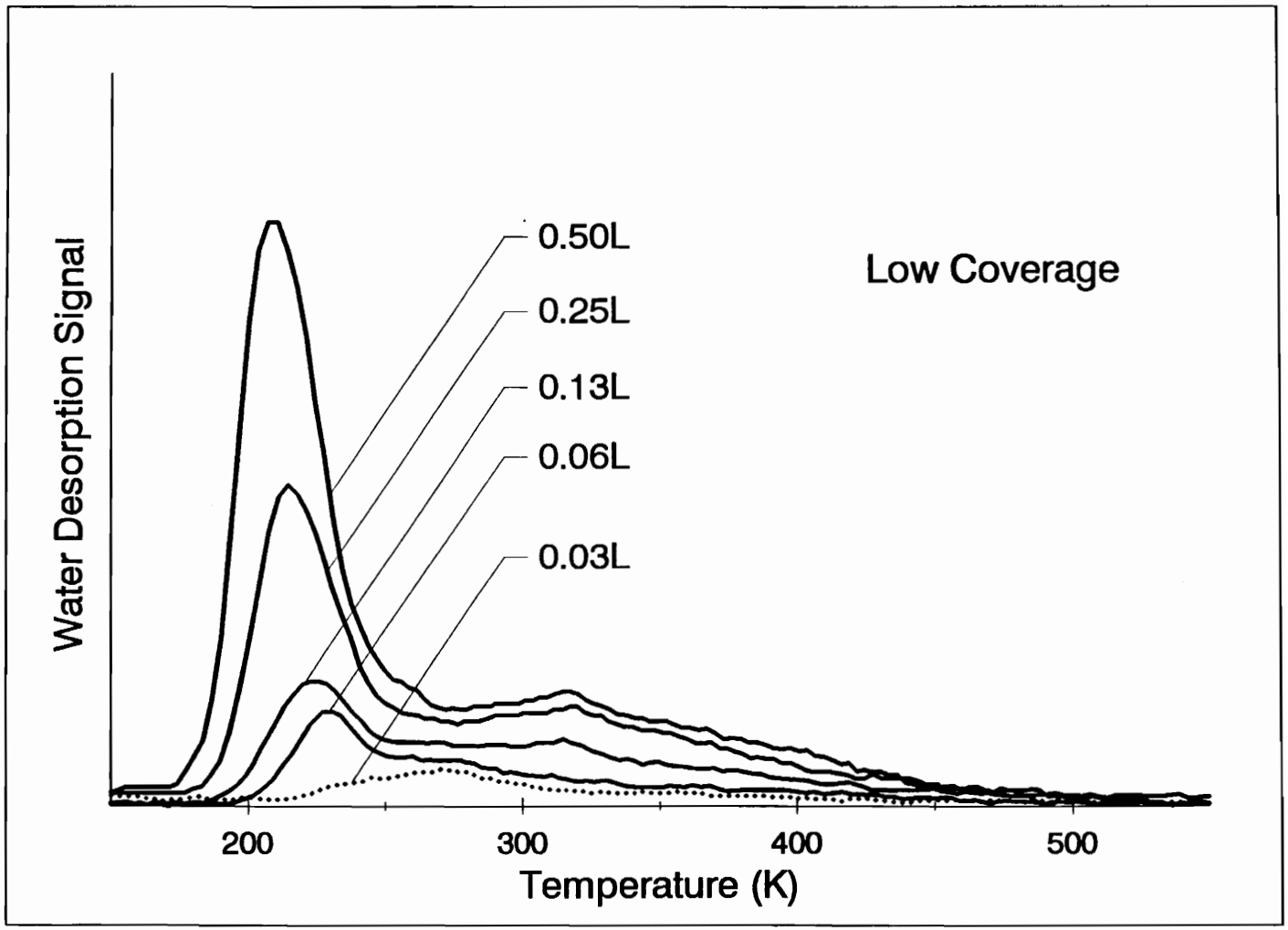

Figure 2.2 Thermal desorption traces for water following adsorption at 110 K on the oxygen-deficient $Cu_2O(111)$ surface.

desorption shows two main features for submonolayer coverages, with the peak temperatures mostly independent of the surface conditions. A low temperature peak is found in the temperature range 190 - 230 K and a higher-temperature feature is seen near 320 K. The amount of water desorption from the high-temperature feature is about 25 ± 5 % for the nearly stoichiometric $Cu_2O(111)$ surface and for the oxygen-deficient $Cu_2O(111)$ surface.

In order to investigate the possibility of changes of the surface composition (number of oxygen vacancies) as a result of water adsorption, the following TDS experiments were conducted. Once the oxygen-deficient surface was prepared, three consecutive TDS traces were run for 0.06 L doses of propene. Then, alternating 0.25 L doses of water and 0.06 L doses of propene were run repeatedly. After the surface was annealed to 1000 K, it was exposed once more to a 0.06 L dose of propene.

The number of oxygen vacancies on the $Cu_2O(111)$ surface seemed not to be sensitive to a large extent to the propene doses. The two peaks seen in TDS spectra (and their relative integrated areas) for a 0.06 L propene dose (solid line in figure 1.2) varied only slightly. This was observed too after the water doses. The propene desorption traces looked much alike before and after 0.25 L of water was dosed. The water traces as well looked similar to one another. Nevertheless, annealing to 1000 K would restore the nearly stoichiometric (1x1) surface. Thus, we observed that water had no effect of reoxidizing or blocking the oxygen vacancies sites.

2.2.2 Ultraviolet Photoelectron Spectroscopy (UPS)

In order to distinguish molecular water adsorption from dissociative water adsorption on $Cu_2O(111)$ surfaces, UPS experiments were conducted following water adsorption at 110 K. As with the TDS experiments, similar results were obtained for both the stoichiometric and oxygen-deficient surfaces.

Figure 2.3 shows the He II UPS data for the nearly stoichiometric surface. Water was initially dosed at 110 K, but UPS spectra were collected at approximately 140 K and 150 K, respectively for the nearly stoichiometric and the oxygen-deficient surfaces, to minimize steady-state charging. Since steady-state surface charging is observed at low temperature, the position of the Fermi level can not be determined. Therefore, the zero binding energy was referenced to the valence band maximum.

The solid N(E) spectrum (figure 2.3 (a)) is characteristic of the clean $Cu_2O(111)$-(1x1) surface. The features between 0 and 8 eV are all derived from the valence band structure of the $Cu_2O(111)$ surface. Features in the photoemission spectrum from 5 to 8 eV are primarily O 2p-derived, while the density of states in the 1-4 eV range is primarily derived from Cu 3d bands [27,28]. The low binding energy feature below 1 eV near the VBM is associated with Cu sp and O p interactions [27].

The dotted N(E) spectrum (fig. 2.3(b)) is representative of a multilayer coverage of water (3 L) on $Cu_2O(111)$. The features at binding

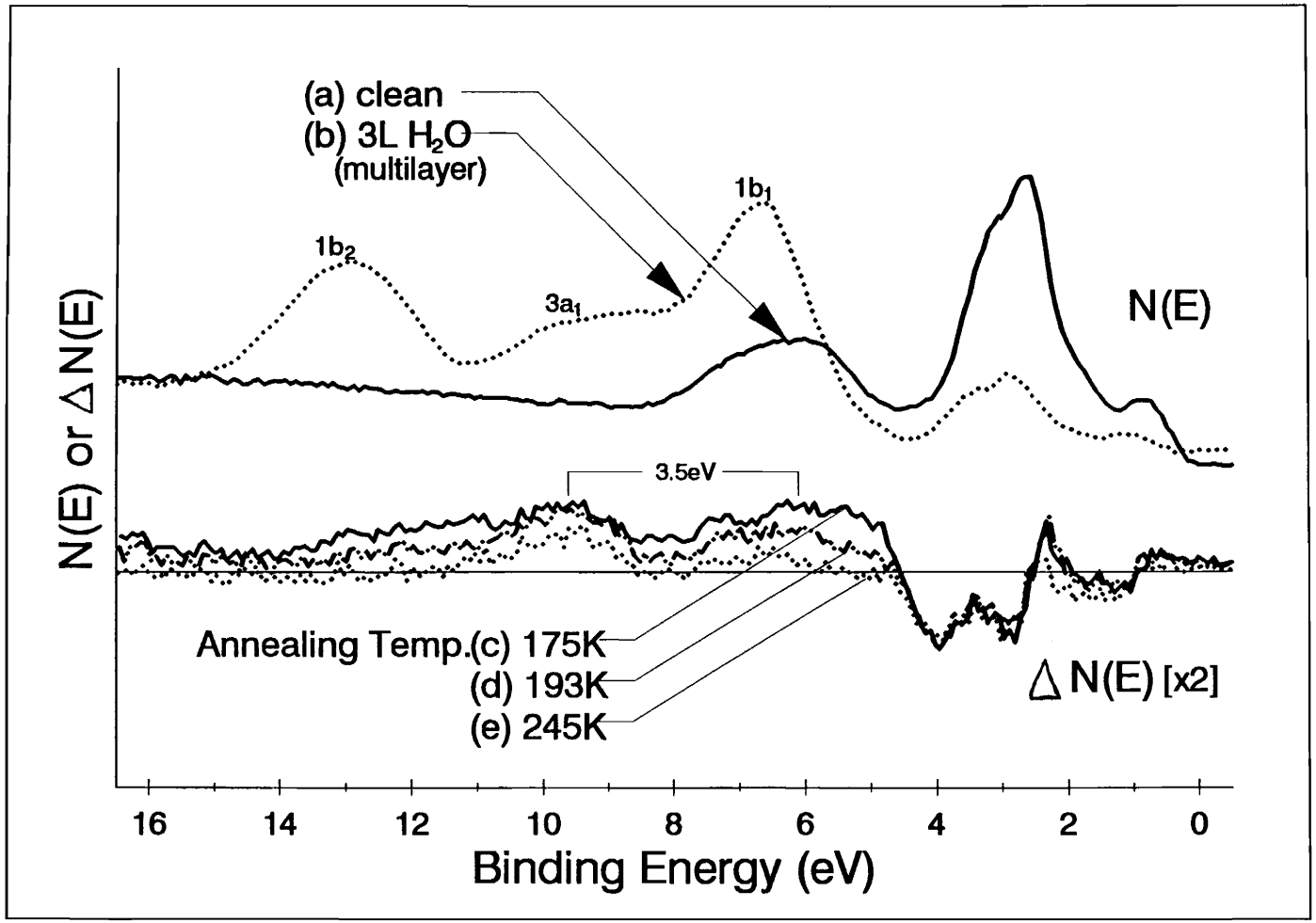

Figure 2.3 HeII spectra for water adsorbed at 110 K on the nearly stoichiometric $Cu_2O(111)$ surface.

energies below 4.5 eV are due to the substrate valence bands, barely observable through the ice multilayer. At binding energies higher than 4.5 eV, the three-peaked emission is characteristic of molecular water. These three peaks are identified as being emissions from the $1b_1$ (B.E. $\simeq$ 6.9 eV), $3a_1$ (shoulder centered at about 9.2 $\pm$ 0.1 eV) and $1b_2$ (B.E. $\simeq$ 13.2 eV) molecular orbitals of water. This spectrum is consistent not only with previous observations of condensed H_2O multilayers on other surfaces [16,13,11,9,10], but also with the gas-phase photoemission of water [29]. The $3a_1/1b_1$ separation for the adsorbed molecular species is about 2.3 eV, very similar to the $3a_1/1b_1$ separation for gas-phase water of 2.2 eV [29].

Difference spectra, $\Delta N(E)$, were obtained by subtracting the N(E) spectrum of the clean surface from the spectrum for the adsorbate covered surface. The thin horizontal line marks the zero-level of the difference spectra. Before generating the $\Delta N(E)$ curves, the spectra were normalized and aligned on the emission from the Cu 3d band feature near the VBM for the clean Cu_2O surface. The alignment was done to account for adsorbate-induced band bending and sample charging. Figures 2.3(c) to 2.3(e) show the variation in the water adlayer caused by heating to successively higher temperatures. For each curve, the sample was held at the indicated temperature (derived from the peak temperatures, Tp, of the TDS experiments) for two minutes before being cooled down near 140 K to collect the UPS data. First, heating to 175 K removes the large contribution of the molecular ice layer. The species associated with the 190 K $\leq$ Tp $\leq$ 230 K and 322 K states observed in TDS are then

remaining on the surface (Figure 2.3(c)). At binding energies higher than 4.5 eV, at least 3 broad features appear in the difference curve at the following binding energies: near 6.1 eV (5.5 eV - 7 eV range), 9.6 eV and 12.8 eV. This last feature, observed near 12.8 eV, is assigned to the $1b_2$ molecular orbital of chemisorbed molecular water (feature near 13 eV in figure 2.3 (c)) because of the similarities in position to that observed on the multilayer spectrum. Further heating to 193 K (figure 2.3(d)) is sufficient to remove most of the lowest temperature chemisorption state (190 K $\leq$ Tp $\leq$ 230 K). We observed decreases in the intensity of the $1b_2$ orbital of chemisorbed molecular water at 12.8 eV as well as of the 6.1 eV feature which includes the $1b_1$ water MO. Further heating to 245 K (figure 2.3(e)) leaves only the adsorbed species associated with the 322 K desorption state. Spectrum 5e shows no feature near 12.8 eV. This feature, assigned to the $1b_2$ MO of water, decreased with heating to finally disappear from the spectrum. The results show that, after annealing to 245 K, there is no remaining molecularly-adsorbed water on the surface. This observation leads to the conclusion that the highest temperature feature is due to dissociation products only. Further heating to 338 K cleans off the surface and no feature are observed. Therefore, the chemisorbed state with the lowest desorption temperature (190 K $\leq$ Tp $\leq$ 230 K) is due to molecular water whereas the 322 K feature is due to recombination of dissociated species.

Previous UPS studies [30,31,32,11] indicate that the formation of OH^- results in two adsorbate molecular orbitals in UPS, the 1π and 3σ, with a separation ranging from 3.3 eV to 4.0 eV [30,31,32]. In figure

2.3(e), after the removal of molecular water, the features centered at 9.6 eV and at 6.1 eV features show a 3.5 eV separation. Hence, the presence of OH^- is likely, with the emission at 9.6 eV being due to the 3σ MO of OH^- and the 6.1 eV being due to the 1π MO of OH^-. Similar results were obtained for the oxygen-deficient surface.

Figure 2.4 shows the variations in surface dipole, $\Delta\chi$, as a function of dose for water exposures on the nearly stoichiometric surface (solid line) and the oxygen-deficient surface (dashed line), near 140 K and 125 K respectively. For a semiconductor, work function changes, $\Delta\phi$, contain contributions from changes in surface dipole, $\Delta\chi$, and changes in surface band bending, $e\Delta V_S$, according to the relationship:

$$\Delta\phi = \Delta\chi - e\,\Delta V_S$$

where V_S is the surface potential associated with the band bending [33]. While charging effects at low temperature make it impossible to accurately determine the changes in work function or band bending with UPS, it is still possible to determine changes in the surface dipole from the He I UPS spectra (not shown) by aligning the Cu_2O valence band features at low binding energies (i.e. those in the 0 to 4.5 eV range which show no significant change in shape) and measuring the variation in the relative position of the vacuum level cutoffs. This procedure accounts for all shifts due to charging and band bending so that the variation in the position of the vacuum level cutoff in a He I UPS spectrum contains only the change in surface dipole, $\Delta\chi$.

For the nearly stoichiometric $Cu_2O(111)$ surface, as shown in figure 2.4, the surface dipole decreases monotonically with H_2O exposure. $\Delta\chi$

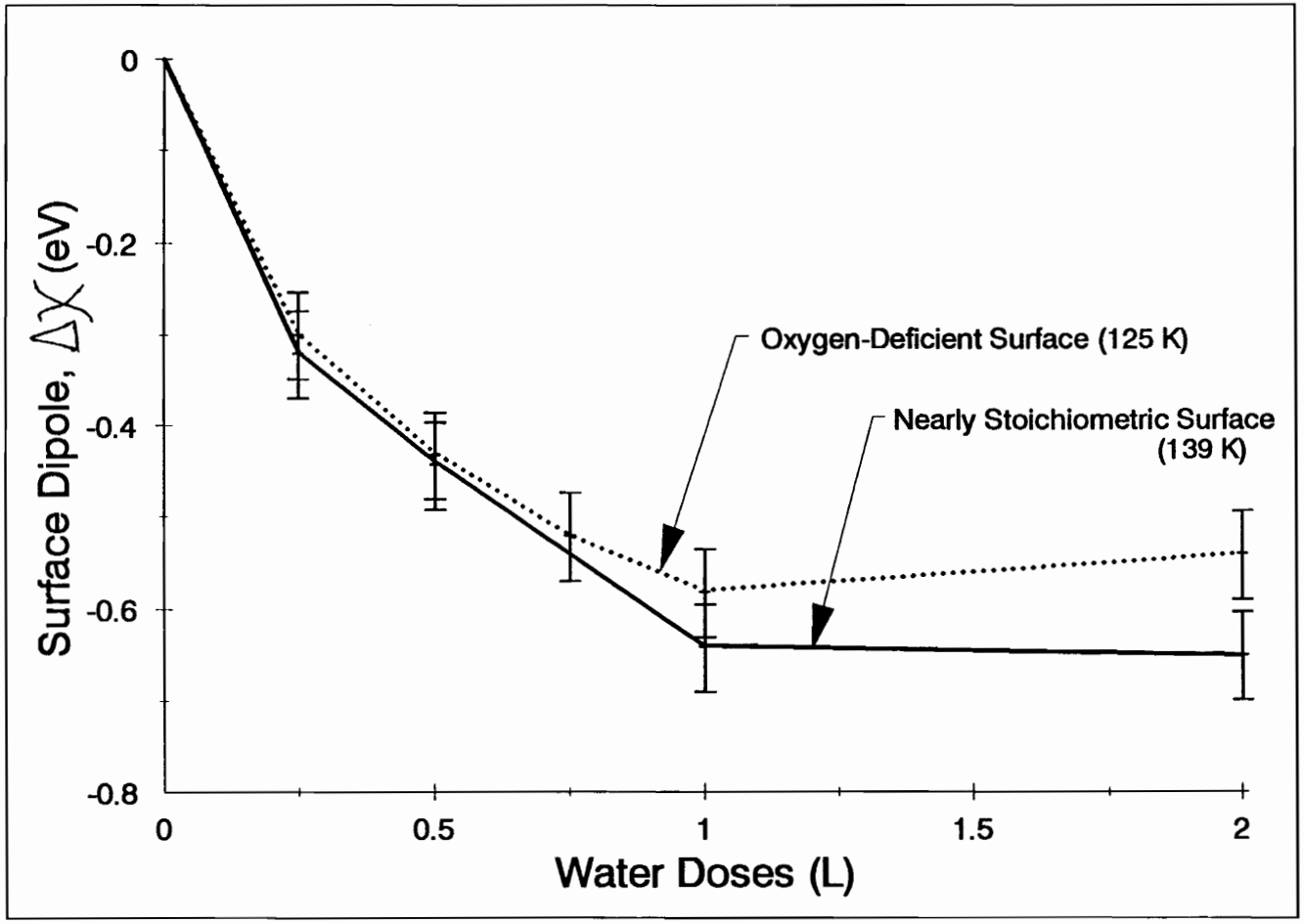

Figure 2.4 Variation of the surface dipole for $Cu_2O(111)$ surfaces

decreases most rapidly for doses below 0.25 L; indeed, it drops down to -0.32 eV. The dipole then decreases more slowly ($\Delta\chi \simeq$ - 0.44 eV for 0.50 L of water, implying a - 0.12 eV change in the surface dipole for the additional 0.25 L of water) with increasing dose for a total change of about 0.65 eV for saturation coverage.

UPS (HeII) following H_2O adsorption at 110 K on the oxygen-deficient $Cu_2O(111)$ surface was similar to that of figure 2.3, showing that on such a defective surface, water adsorption is molecular and dissociative. Dissociative adsorption, as stated earlier in section 2.2.1.2, represented 25 ± 5 % of a monolayer.

The change of surface dipole for the oxygen-deficient surface at 125 K is also shown in figure 2.4. Within the error-bars (evaluated to be about ± 0.05 eV from the data manipulation, i.e. normalization, alignment of the Cu 3d band emission as well as alignment of the vacuum level cutoff), the variation of surface dipole with water dose for the oxygen-deficient surface shows the same trend to that observed on the nearly stoichiometric surface.

While the amounts of surface defects created by exposures to dissociated H_2 varied somewhat from run to run, the results demonstrate that the introduction of oxygen-vacancies does not seem to significantly influence water adsorption. Thus, it is concluded that dissociative adsorption on the $Cu_2O(111)$ surface is not enhanced by the presence of threefold sites of singly-coordinate Cu^+ cations at oxygen vacancies.

2.3 Discussion

The TDS results can be explained as follows. The feature in the temperature range 190 K $\leq$ Tp $\leq$ 230 K is identified as molecular water based on the low TDS peak temperature as well as on the observation of molecular water in the UPS spectrum for temperatures below 230 K. The decrease in Tp with increasing coverage for this chemisorbed molecular water feature in TDS is similar to that observed on the well-defined single-crystal $Cu_2O(100)$ surface [16]. This observation though differs from previous studies on a number of atomically smooth metal surfaces, Ni(111) [34,35], Rh(111) [23], Ru(001) [22], Pt(111) [7], Cu(110) [36] and Pd(100) [21], for which a shift to higher temperature with increasing coverage is observed. For these metals, since the experimental observation can not be explained by a simple first-order desorption kinetics model, two models based on the lateral interactions between H_2O molecules in the adlayer have been proposed. One model assumes first order desorption kinetics and states that attractive interactions are of a few kJ/mol between water molecules, a value significantly smaller that accepted for a single hydrogen bond in water (15 - 25 kJ/mol) [34,35]. A second model suggests that desorption from the perimeter of hydrogen bonded clusters or islands on the surface decreases the desorption order to less than one [7]. For $Cu_2O(111)$, such lateral interactions between water molecules in the adlayer do not appear to influence the desorption

kinetics. Assuming normal first-order kinetics and applying the Redhead equation [26] gives a range of activation energies for desorption of about 14.2 kcal/mol (59.3 kJ/mol) at low coverages to 11.6 kcal/mol (48.5 kJ/mol) at near monolayer coverages. The values compare reasonably with the 10 to 15 kcal/mol (40 to 65 kJ/mol), range identified for the molecular chemisorption bond strength on metal surfaces [10], as well as for the heat of adsorption on oxide powders (40 to 60 kJ/mol). Therefore, the absence of influence of the attractive lateral interactions observed in the desorption of molecularly adsorbed water on $Cu_2O(111)$ can not be assigned to an increased strength of the H_2O - substrate bond, expected to reduce the mobility of molecular water. Also, in the vibrational spectroscopic studies of $Na_{0.7}WO_3(001)$ [37] and $SrTiO_3(100)$ [38], the absence of apparent hydrogen bonding between H_2O molecules was explained by the fact that adsorption occurs at surface cations, hence overriding the tendency for clustering observed on metals. Zwicker and Jacobi [39] showed that, on ZnO surfaces, molecular water binds more strongly to cation sites than to anion sites in TDS studies. However, clustering is still thought to happen with bonding to zinc sites. For $Cu_2O(111)$, as stated by Schulz and Cox for $Cu_2O(100)$ [16], the similarity in the activation energy for desorption of molecular water with that seen on metal surfaces suggests that either the surface structure (and not a high H_2O - substrate bond strength) hinders surface diffusion (hence clustering), or that the surface controls the local structure of the molecular adsorbate, thus preventing any hydrogen bonding between adjacent water molecules. But, since water molecules are thought to bind at surface

cations, there is still a possibility of hydrogen-bonding with neighboring surface oxygen anions. Vibrational spectroscopies are necessary to identify the importance, if any, of hydrogen bonding to lattice oxygen anions and/or between water molecules.

From the combination of TDS and UPS, it is clear that the feature observed near 320 K which broadens to about 450 K - 500 K is due to dissociated water. The indication of OH^- groups on the $Cu_2O(111)$ surface by UPS after removal of molecular water leads to the conclusion that water dissociation forms surface hydroxyl groups, as observed previously on various metal surfaces [21,40]. OH^- disproportionation to form water has been proposed on the following oxides: NiO(100) [31], V_2O_3 [32], Ti_2O_3 [11], $SnO_2(110)$ [25] and $Cu_2O(100)$ [16]. For the latter, water desorption via recombination was observed near 300 K and assigned to OH disproportionation, and 465 K associated with a first-order rate limiting step [16]. On $Cu_2O(111)$ surfaces, no high-temperature feature in the TDS traces was clearly resolved near 450 K as was seen on $Cu_2O(100)$ [16], $SnO_2(110)$ [25] or $TiO_2(110)$ [12]. A small, broad feature was observed: it appears to be associated with first order kinetics rather than second order kinetics. This observation suggests that the rate-limiting step on $Cu_2O(111)$ may not be OH disproportionation but may be a first-order decomposition of OH^- groups to form water. A possible reaction scenario could involve a first-order, rate-limiting decomposition of OH to give hydrogen which quickly reacts with other OH groups to form water. This is consistent with the temperature range where the broad feature is observed. Schulz and Cox [16] previously observed a first-order kinetics

process at higher temperature on $Cu_2O(100)$ as well. However, on $Cu_2O(100)$, the high-temperature feature was clearly resolved as a independent peak at 465 K. The behavior of Cu_2O surfaces appear to be different from a (100) to a (111) orientation concerning their respective abilities to decompose oxygenated surface intermediates: alkoxide groups are also more readily decomposed on the (111) surface than on the (100) surface [41,42].

The difference curves in UPS allow us to clearly distinguish between molecular and dissociated water, with an apparent OH^- contribution for dissociated water. However, it is difficult to specifically identify the relative contribution of the possible different products produced by water dissociation, atomic oxygen, atomic hydrogen or hydroxyl groups. A comparison of the rapid decrease in the surface dipole changes in figure 2.4 at low coverages associated with dissociatively adsorbed water with that expected for atomic hydrogen adsorption and for atomic oxygen could provide some insight into the type of dissociation products formed upon water adsorption. For atomic hydrogen adsorption, the surface dipole, χ, is expected to decrease according to photoemission experiments of predissociated hydrogen adsorption on $Cu_2O(100)$ surfaces [16,6] whereas under atomic oxygen adsorption, χ is expected to increase [16,10]. The presence of such negative species on the surface causes the surface dipole to increase. Also, the presence of hydroxyl groups on the surface should reduce the surface dipole as observed on other oxides surfaces such as Ti_2O_3 [11], V_2O_3 [32] and NiO [31]. The decreased surface dipole observed on figure 2.4 at low doses is consistent with OH

bonding through the oxygen atom with the dipole (O-H bond axis) oriented away from the surface [31]. At higher coverages where molecular water is the primary adsorbed species, the decrease of χ with increasing doses in figure 2.4 is consistent with expectations. Molecular water bound to a surface cation with the oxygen end down and hydrogen oriented away from the surface has a positive net dipole oriented away from the surface and thus is expected to decrease the surface dipole [10]. Since both molecular and dissociated water are present on the surface, figure 2.4 itself does not allow us to clearly identify the relative contribution in the surface dipole change of each species. Atomic hydrogen and oxygen can not be completely ruled out.

The shape of the 320 K feature in the TDS traces suggests that there may be more than just one contribution to the desorption signal. For 0.03 L and 0.06 L of water, it looks like a feature near 280 K grows in, but it is not as well resolved as the molecular water desorption peak near 230 K. For larger doses, this feature is dominated by the other desorption signals. The constant peak temperature with increasing coverage of the feature near 320 K was attributed to a first-order decomposition of hydroxyl groups. Nevertheless, its shape is not typical of a first-order desorption signal. Therefore, other recombination pathways in the high-temperature tail of this feature, OH disproportionation as an example, can not be ruled out. Indeed, recombination via disproportionation of hydroxyl groups has been observed on smooth metal surfaces. This desorption observed near 320 K on $Cu_2O(111)$ is in the range (200 - 360 K) associated with the recombination via disproportionation of hydroxyl

groups from smooth metal surfaces [10]. Among the transition metals, there is a good evidence for dissociation of water even at temperatures lower than 100 K on Ti(001) [9], Cr(110), Mn films, MO films and Fe(100) [10]. On oxygen predosed metal surfaces, Ag(110) and Ag(311) as well as on Ni(110) [40], H_2O is observed to desorb due to recombination of OH_a at 320, 310 and 360 K respectively. Benndorf *et al.* [13] also observed that water evolution from recombination of dissociation products is typically complete by at least 350 K. This is consistent with our discussion on the possible contributions observed in the 320 K TDS feature.

The observation that the coverage of dissociated water does not change significantly between the nearly stoichiometric and the oxygen-deficient surfaces demonstrate that oxygen vacancies on the $Cu_2O(111)$ surface do not significantly influence the dissociation process. This is different from previous studies, according to which defects are, in general, thought to increase the ability of the surface to adsorb and/or dissociate water. Thiel and Madey recall that water is very efficient in hydroxylating surfaces on powders of common oxides such as Al_2O_3 due to the defects sites or facet edges [10]. On $Ti_2O_3(10\underline{1}2)$ [11], $TiO_2(110)$ [12], $TiO_2(100)$ [13] or MgO(100) [14], the defects created on the surface affect the dissociative adsorption process: defect-free surfaces of these oxides do not dissociate H_2O to a significant extent. On $Cu_2O(111)$, we observed that there were no significant differences between the nearly stoichiometric and oxygen-deficient surfaces. Our results could indicate that local atomic structure does not play a significant role in the dissociation of water on $Cu_2O(111)$ surfaces. It does not appear to be a

peculiarity of the (111) crystallographic orientation since Schulz and Cox [16] obtained similar results with the ordered and defective $Cu_2O(100)$ surfaces.

The observation that about 0.25 of a monolayer of water dissociates on $Cu_2O(111)$ regardless of surface condition is fairly similar to that observed on $Cu_2O(100)$ [16]. Nevertheless, it differs from the dissociative adsorption of water on $TiO_2(110)$ [12]. Indeed, Hugenschmidt *et al.* [12] observed that water dissociation was enhanced by oxygen vacancies on the surface.

Our results on the oxygen-deficient surface showed that upon water adsorption, the concentration of surface oxygen vacancies was unaffected, indicating little or no reoxidation of oxygen vacancies with water. This behavior is different from that observed on the same surface for ammonia [43], where NH_3 molecules were observed to block the oxygen vacancies sites and thus to modify the local surface properties of the defect.

2.4 Conclusions

Adsorption of water on two types of $Cu_2O(111)$ surfaces was studied; water was the only product observed. Desorption of water occurs at three temperatures: ice multilayer desorption near 180 K, molecular desorption at 190 K - 230 K and desorption near 320 K mainly attributed to decomposition of OH groups. The amount of dissociation (25 ± 5 %) and the desorption kinetics were similar on the stoichiometric and the oxygen-deficient surfaces. The presence of oxygen vacancies does not enhance dissociative water adsorption on $Cu_2O(111)$ surfaces.

CHAPTER 3

Carbon Monoxide Adsorption on $Cu_2O(111)$ Single Crystal Surfaces

3.1 Introduction

Research on adsorbed CO represents well many of the key advances which characterize the first thirty years of development of surface science [51]: CO can represent the focal point for the development of a number of key experimental methods for surface science. Being a simple molecule with the highest dissociation energy of any molecule, it is a good test molecule for new surface measurement techniques, low temperature STM as an example [51]. It constitutes a bridge between surface chemistry on transition metal surfaces and the field of organometallic chemistry through the metal carbonyls, where the carbonyl ligands often closely resemble chemisorbed CO species on transition metal surfaces. It is also one of the centrally important molecules in heterogeneous catalysis. The production of synthetic fuel and many useful organic molecules depends on the catalytic behavior of the adsorbed CO molecule [51].

There has been much discussion in the heterogeneous and homogeneous catalysis, theoretical and surface science literature concerning the nature of active sites, the intermediates involved and the mechanism of methanol synthesis from CO and H_2. Recently, the nature of active copper species in Cu/ZnO methanol synthesis catalyst has been the subject of much debate [45,46]. Copper(I) cations stabilized by substitutional dissolution in the surface of the ZnO lattice have been suggested as one of the possible species responsible for the unique selectivity of this catalyst [45]: the Cu(I) sites appear to be the active centers for the high activity for methanol synthesis of the Cu/ZnO catalysts [46]. Cu^+ sites appear to bind CO more strongly than either Cu metal or ZnO [45]. A comparison of the interaction of CO with Cu^+ cations on the extended $Cu_2O(100)$ surface (Cu^+-terminated) and on the Cu-deposited ZnO single-crystal surface suggested that variations in the local site geometry could also account for significant differences in the mode of CO binding to surface cations [46]. The standard model for CO bonding to transition metals was proposed by Blyholder in 1964 [51] in terms of donor-acceptor bonding between CO and any surface: various sites could donate more or less electrons to the antibonding CO ($2\pi^*$) levels to achieve the desired C-O bond strength.

CO adsorption studies have been reported for a wide variety of surfaces starting as early as 1922 with Langmuir who studied the catalytic reaction of CO and O_2 over Pt [51]. However, CO adsorption on oxide single-crystal surfaces has shown a different binding behavior than that observed for CO chemisorption on metals. The heat of adsorption for CO

on different surfaces can be an indicator of such behaviors. The heat of adsorption for CO on pure ZnO is about 12 kcal/mol [45]. The heat of adsorption for CO on Cu metal varies as a function of surface crystallographic orientation and coverage, with maximum reported values for different surfaces ranging from 12.5 to 16.6 kcal/mol [45]. For CO on CuCl(111), the heat of adsorption was found to be 23 ± 2 kcal/mol. Reported values for the heat of adsorption for CO attributed to dispersed Cu^+ cations in a ZnO matrix are 18.2 and 21 ± 2 kcal/mol (experimental values) [50] and 22.4 kcal/mol (theoretical) [45]. On $Cu_2O(100)$ single-crystal surfaces, the heat of adsorption was reported as 16.7 kcal/mol in the limit of zero coverage [45].

A nearly stoichiometric $Cu_2O(111)$ surface exposes triply-coordinate oxygen anions in the outer atomic layer, as well as singly- or doubly-coordinate copper cations in the second atomic layer. However, oxygen vacancies on the surface give rise to a threefold site of singly-coordinate Cu^+ cations in the second atomic layer. The adsorption of CO on $Cu_2O(111)$ surfaces has been studied to complement the previous studies of CO adsorption on Cu^+ sites. Do the local coordination environment associated with the surface crystallographic orientation affect CO adsorption on Cu_2O single-crystal surfaces? What type of bonding interactions does CO adsorption on $Cu_2O(111)$ surfaces give rise to? Is σ-bonding dominant for CO on $Cu_2O(111)$? Is π-backbonding (if any) significant?

3.2 Results

3.2.1 Thermal Desorption Spectroscopy

Variations in the adsorption of CO were examined on the surfaces described above. The desorption behavior of CO appears to be similar on both surfaces.

3.2.1.1 Nearly stoichiometric surface

The clean surface was exposed to CO at the lowest possible temperature, 105 K, and then heated linearly at 2 K/s to 700 K. Only CO was observed as a desorption product in TDS following CO adsorption. O_2 and CO_2 were not observed as desorption products. No residual surface carbon was detected with XPS following thermal desorption. Recombination of atomic oxygen occurs between 400 and 500 K on $Cu_2O(100)$ [18], while surface carbon undergoes a "burn-off" reaction to CO and CO_2 at temperatures above 500 K [52]. Since no products are observed for either of these reactions, no dissociative adsorption occurs under the conditions used in this study.

The coverage dependance of the CO desorption traces for the nearly stoichiometric surface following adsorption at 105 K is illustrated in figure 3.1. The left panel shows the low coverage regime (doses less than 0.5 L)

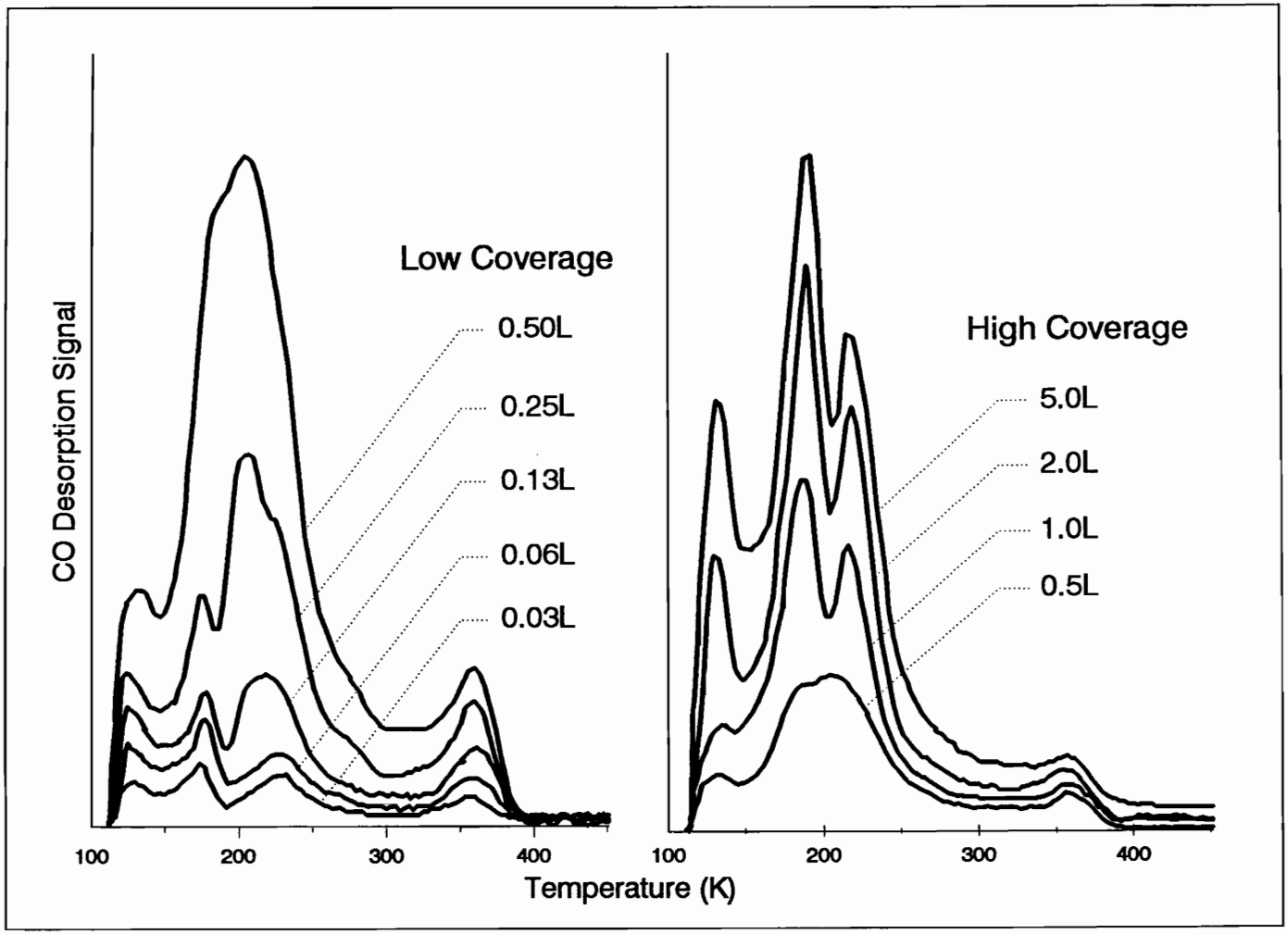

Figure 3.1 Thermal desorption traces for CO following adsorption at 105 K on the nearly stoichiometric $Cu_2O(111)$ surface

and the right panel shows the high coverage regime (doses up to 5 L). At the lowest dose investigated, 0.03 L, four CO features were observed at 128 K, 176 K, 230 K and 358 K. Larger doses up to 0.25 L resulted in increased intensities and shifts to lower temperatures for all features but the highest-temperature one at 360 K. The 230 K feature shifted to 227 K for 0.06 L. For 0.13 and 0.25 L of CO, a feature grows in at 209 K. The two features observed at 209 and 227 K for 0.25 L of CO overlap near 206 K for 0.5 L of CO. This broad feature, for a 0.5 L dose, dominates the desorption traces; the low- (134 K) and high-temperature (360 K) features make only a small contribution to the overall CO signal. The other features (122 K, 176 K and 360 K) grow in with larger doses up to 0.25 L. For doses larger than 1 L, the 206 K feature is resolved again into two features: 188 K, which shifts slightly to higher temperature for 5 L of CO, and 216 K.

The Redhead equation [26] can be used to estimate the activation energy for desorption, E_d, for a first-order molecular desorption process. The 360 K feature appears to be first-order, identified by the nearly constant peak temperature with changing coverage [26] for doses up to 5 L. Assuming a normal pre-exponential of 10^{13} s^{-1} gives a value of 22.5 ± 1 kcal/mol for the maximum activation energy for desorption of this high-temperature feature. As noted in section 1.3, the heating rate was kept intentionally low (2 K/s) to avoid the possibility of thermal fracture of the sample. Hence, no attempt was made to independently determine the pre-exponential via the method of heating rate variation [53]. Calculations of E_d using a previously defined range of pre-exponential (1 x 10^{13} to 5 x

10^{13} s^{-1}) for Cu(110) [45] gives a maximum increase in E_d of less than 1 kcal/mol within the quoted uncertainty in our value. Ranges of first-order E_d for the different features observed in TDS (assuming $\nu = 10^{13}$ s^{-1}) are 12.7 - 14.2 kcal/mol (206 - 230 K), 10.7 - 11.6 kcal/mol (176 - 190 K), and $\leq$ 8.1 kcal/mol (132 K and below).

3.2.1.2. Oxygen-deficient surface

The coverage dependance of the CO traces for the oxygen-deficient $Cu_2O(111)$ surface is illustrated on figure 3.2. The left panel shows the low coverage regime (doses less than 0.5 L) and the right panel shows the high coverage regime (doses up to 5 L). The TDS traces for CO adsorption on the oxygen-deficient surface look similar to the TDS traces for CO adsorption on the nearly stoichiometric surface. For 0.25 L of CO, four features are clearly observed: at $\leq$130 K, 177 K, 210 K, and 360 K. Increasing coverage resulted in increased TDS features intensities. The 210 K feature overlaps the 177 K feature: we observe a broad peak at 209 K for 0.5 L of CO. This feature, for a 0.5 L dose, dominates the desorption traces; the low-($\leq$130 K) and the high-temperature (360 K) features made only a small contribution to the overall CO signal. For 1 L, the 209 K feature was resolved as two separate features again, at 187 K and 220 K. This last feature shifted to 215 K for 5 L of CO. As observed on the nearly stoichiometric surface, all features but the 360 K peak increased without saturation with increasing coverage. The main difference in the TDS traces for the nearly stoichiometric and the

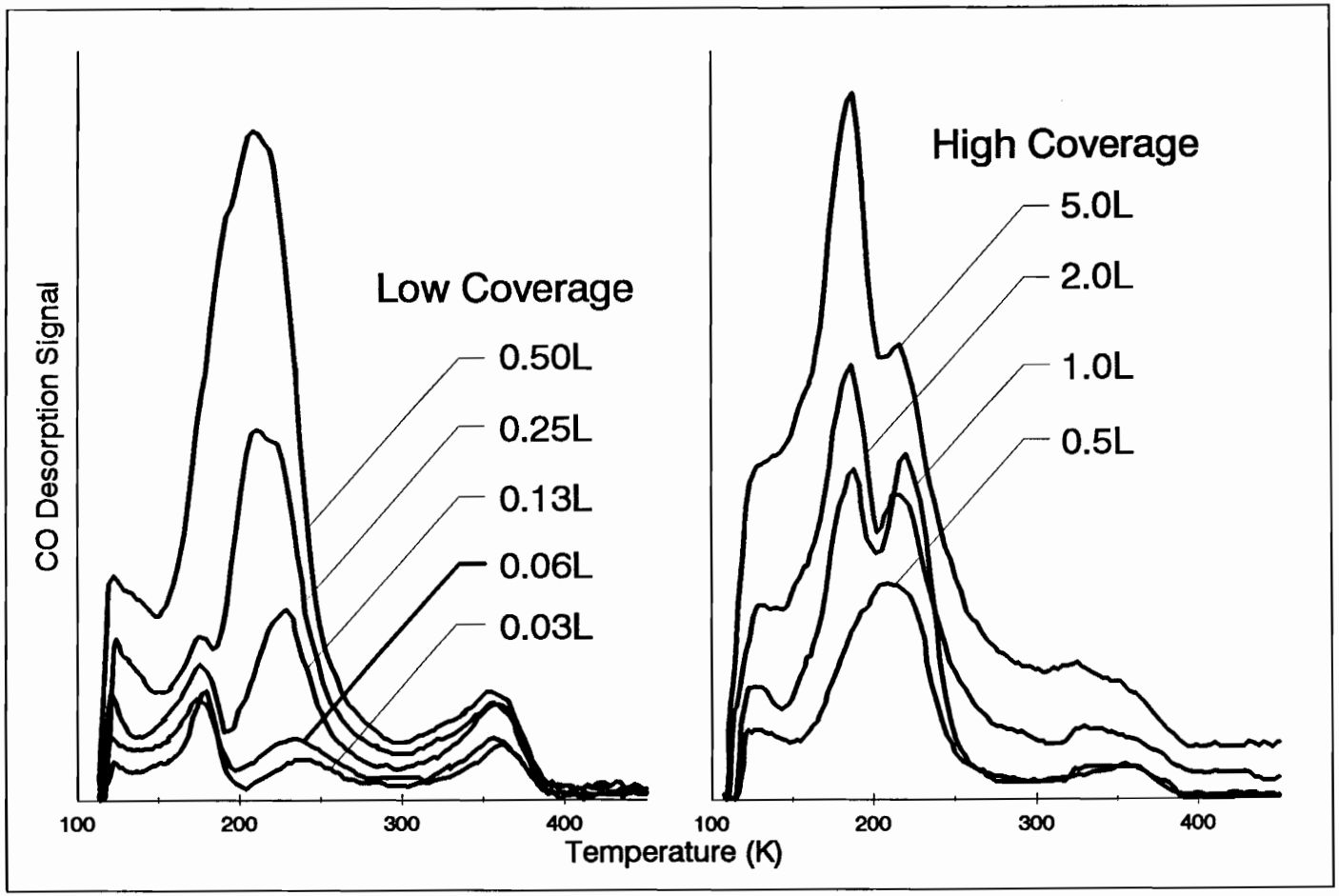

Figure 3.2 Thermal desorption traces following CO adsorption at 105 K on the oxygen-deficient $Cu_2O(111)$ surface

oxygen-deficient $Cu_2O(111)$ surfaces is seen for the 0.03 L and 0.06 L CO doses. The feature observed on the nearly stoichiometric surface at 230 K shifted to higher temperatures, 245 K for CO adsorption on the oxygen-deficient surface. Also, for 0.13 and 0.25 L doses, the 227 - 230 K feature is not observed to result from two different contributions, as we saw for the nearly stoichiometric surface. With the assumption that the 350 - 360 K desorption feature is first-order along with the Redhead equation [3] (see section 2.2.1), the activation energy for desorption associated with this feature is found to range 21.9 - 22.5 kcal/mol, very close to the range of activation energies for desorption associated with CO adsorption on the nearly stoichiometric surface. Ranges of E_d for the other TDS features observed in TDS (assuming $\nu = 10^{13}\ s^{-1}$) are 12.9 - 15.1 kcal/mol (210 - 245 K), 10.8 - 11.4 kcal/mol (177 - 187 K), and $\leq$7.9 kcal/mol (Tp: 130 K and below).

The CO uptake at 105 K as a function of dose is shown in figure 3.3 as determined from the integrated CO desorption signal in TDS. For doses up to 0.5 L for the nearly stoichiometric surface and 0.2 L for the oxygen-deficient surface, the data are linear, demonstrating a constant sticking coefficient at low coverages. As doses increase to 5 L, the features do not saturate. Hence, saturation coverage is not achieved for doses smaller than 5 L. In a previous study [45], Schulz and Cox showed that doses above 2000 L were required for saturation coverage of CO on a $Cu_2O(100)$ surface. For doses up to 0.25 L, the CO uptake for both surfaces is similar. For larger doses, the CO uptake on the nearly stoichiometric surface is higher ($\approx$ 20 $\pm$ 5 %) than that on the

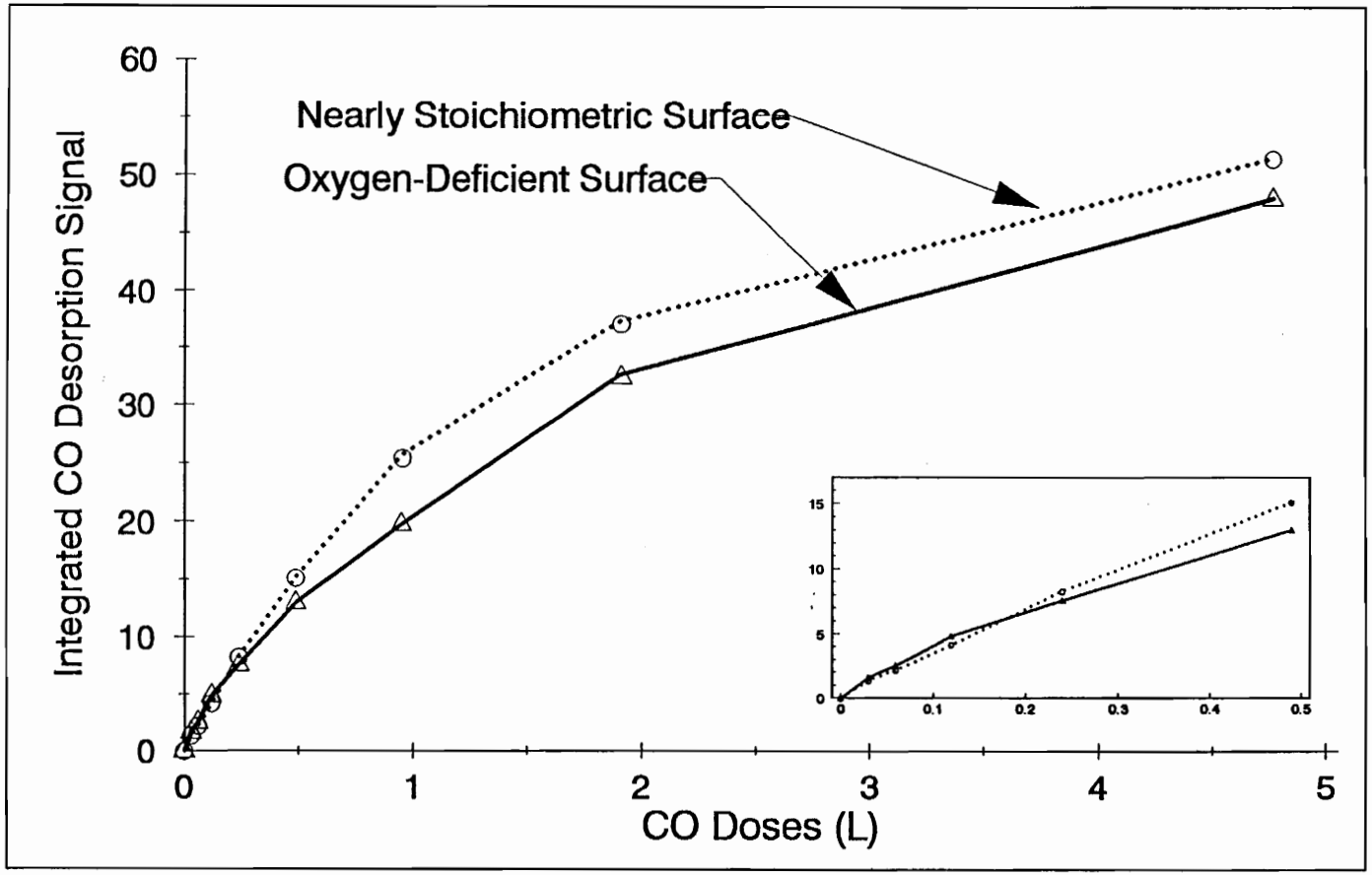

Figure 3.3 Variation of the coverage of CO adsorbed at 105 K on the nearly stoichiometric and on the oxygen-deficient $Cu_2O(111)$ surfaces as a function of CO exposure

oxygen-deficient surface. This is very unlikely to be due to some CO molecules which stick to the surface since no surface carbon "burn-off" is observed in TDS. This could suggest that, for a given dose, the coverages of CO on the nearly stoichiometric and on the oxygen-deficient are different, i.e., the sticking coefficient is slightly different.

The TDS results on $Cu_2O(111)$ surfaces demonstrate that CO desorption shows four main features, with the peak temperatures mostly independent of the surface conditions. Two-low temperature peaks are found under 132 K and in the 176 K - 190 K range, one intermediate-temperature peak is seen in the temperature range 206 K - 230 K and a higher-temperature feature is observed near 360 K. There is no apparent significant difference in between the stoichiometric and reduced surfaces.

In order to investigate the possibility of changes of the surface composition (number of oxygen vacancies) as a result of CO adsorption, once the oxygen-deficient surface was prepared, 0.06 L doses of propene alternating with increasing doses of CO were run. The number of oxygen vacancies on the $Cu_2O(111)$ surface seemed to be sensitive to the amount of CO dosed on the surface. The peak temperatures and the relative integrated areas of the two features observed for 0.06 L of propene on $Cu_2O(111)$ surfaces were affected by CO exposure of the surfaces. Indeed, as shown on figure 3.4, before the surface was exposed to 0.03 L of CO, the desorption trace for 0.06 L of propene (trace (a)) showed two peaks of the same height, characteristic of the oxygen-deficient surface (see section 2.2.1), respectively at 254 K and 337 K. After TDS was run

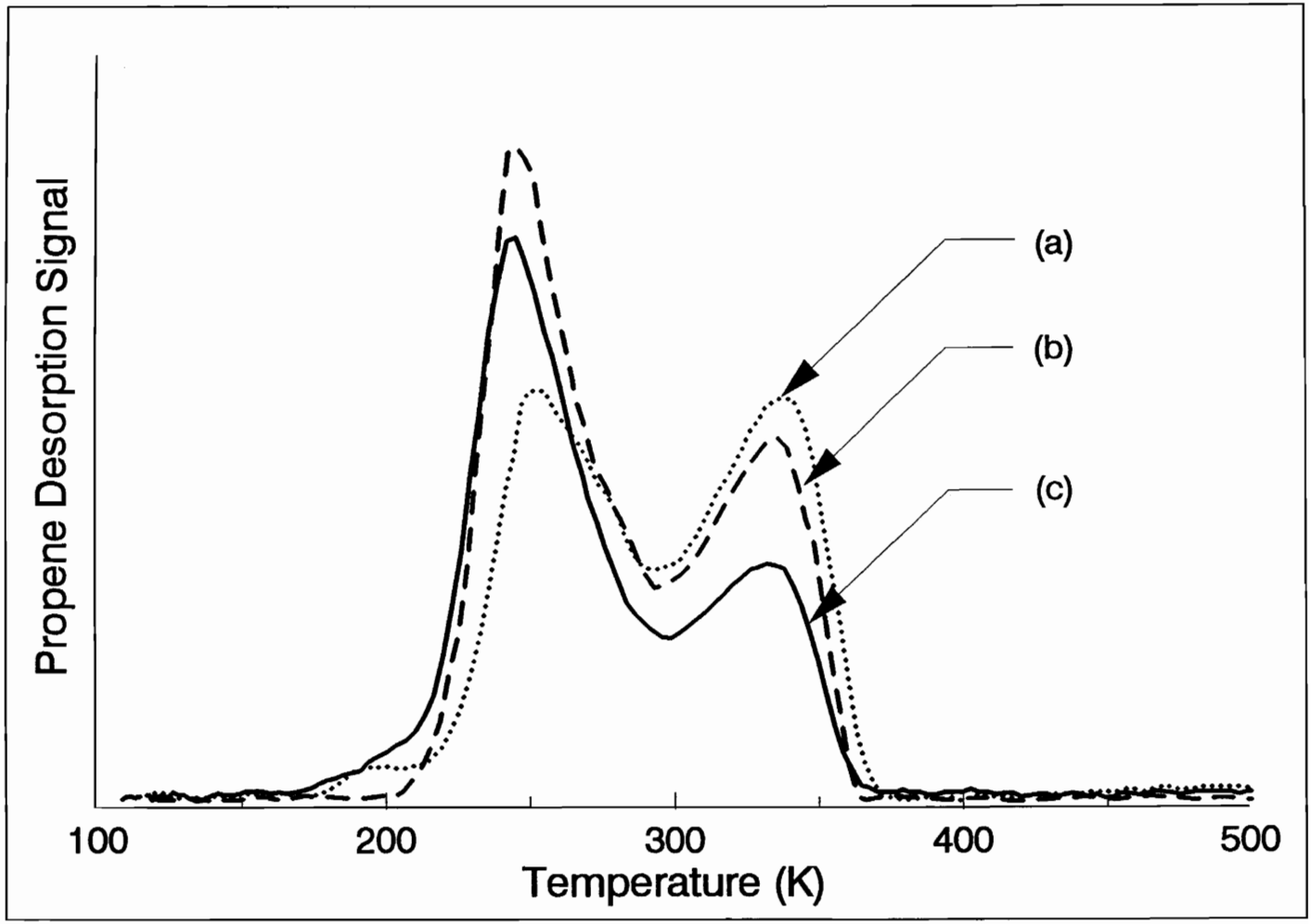

Figure 3.4 Thermal desorption spectra of 0.06 L propene doses on the oxygen-deficient surface, alternated with TDS experiments for increasing doses of CO.

for a 0.03 L dose of CO, the propene desorption trace (trace (b)) changed: the high-temperature feature (337 K), reported in previous studies as being representative of the number of oxygen vacancies on the surface, decreased significantly relative to the low temperature feature, which, itself, shifted slightly to lower temperature (245 K). After several TDS runs for successive and increasing doses of CO up to 2 L, the propene desorption trace (trace (c)) showed that the higher temperature peak decreased even more relatively to the low-temperature feature. Even though oxygen vacancies were still present on the surface, there was only a limited number of them. Thus, CO is seen to have some effect on blocking, reoxidizing, or otherwise altering the chemisorption properties of oxygen vacancies sites although there is no apparent CO dissociation. This effect is not understood. Similar results were observed with ammonia on the oxygen-deficient $Cu_2O(111)$ surface [43]. By contrast, water, as mentioned in section 2.3, was not observed to have any effect of reoxidizing or blocking the oxygen vacancies sites.

3.2.2 Ultraviolet Photoelectron Spectroscopy (UPS)

UPS (He I and He II) experiments were conducted following CO adsorption at 105 K. Even though CO was dosed near 105 K, all UPS spectra were collected at approximately 120 K. Since steady-state surface charging was observed at low temperature, the Fermi level could not be determined and therefore the zero binding energy was chosen at the

valence band maximum.

Figures 3.5 and 3.6 show the variation in the He II energy distribution curves (EDCs) and difference curves for doses of 0.25 L, 1 L and 5 L at 120 K on the nearly stoichiometric surface. Difference spectra, $\Delta N(E)$, were obtained by subtracting the N(E) spectrum of the clean surface from the spectrum for the adsorbate covered surface. The thin horizontal line marks the zero-level of the difference spectra. Before generating these $\Delta N(E)$ curves, the spectra were normalized and aligned on the emission from the Cu 3d band feature near the VBM for the clean Cu_2O surface. This was done to account for adsorbate-induced band bending and sample charging. The features observed in the EDCs and difference curves are similar for CO dosed at 105 K, or for an adsorbed layer heated sequentially to remove the different desorption states; i.e., there is no apparent interconversion between electronically distinguishable forms of adsorbed CO due to heating.

A number of features may be observed in the EDCs in figure 3.5. The features between 0 and 8 eV are all derived from the valence band structure of the $Cu_2O(111)$ surface. Features in the photoemission spectrum from 5 to 8 eV are primarily O 2p-derived, while the density of states in the 1-4 eV range is primarily derived from Cu 3d bands [27,28]. The low binding energy feature below 1 eV near the VBM is associated with Cu sp and O p interactions [27].

Traces (b), (c) and (d) are representative of adsorbed CO following 0.25 L, 1 L and 5 L doses, respectively. The features at binding energies below 4.5 eV are due to the substrate valence bands. At binding energies

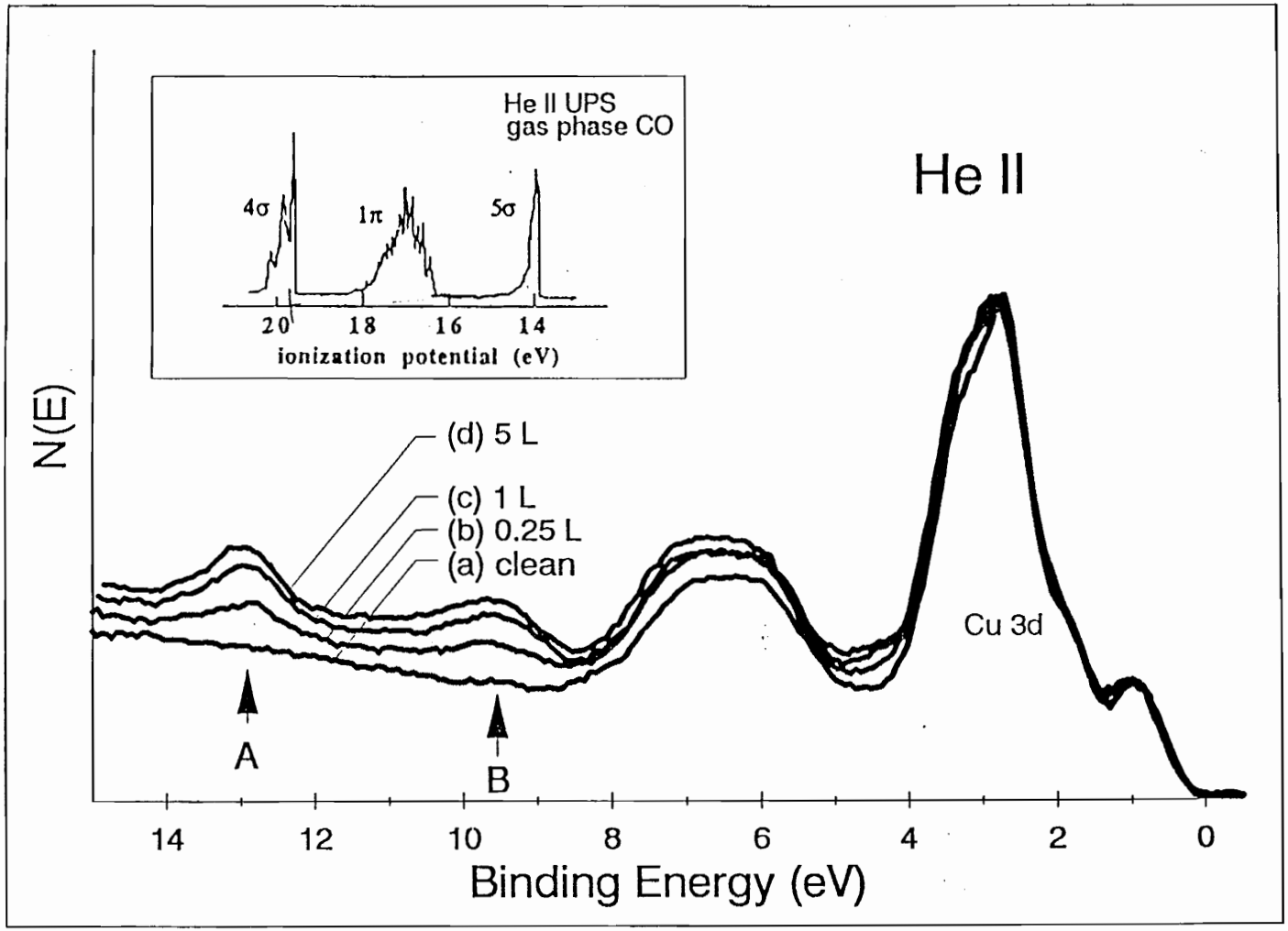

Figure 3.5 He II UPS spectra of CO adsorbed on $Cu_2O(111)$-stoichiometric as a function of increasing coverage at 105 K. The data have been normalized on the Cu 3d band. The He II spectrum of gas-phase CO [46] is included at the top left

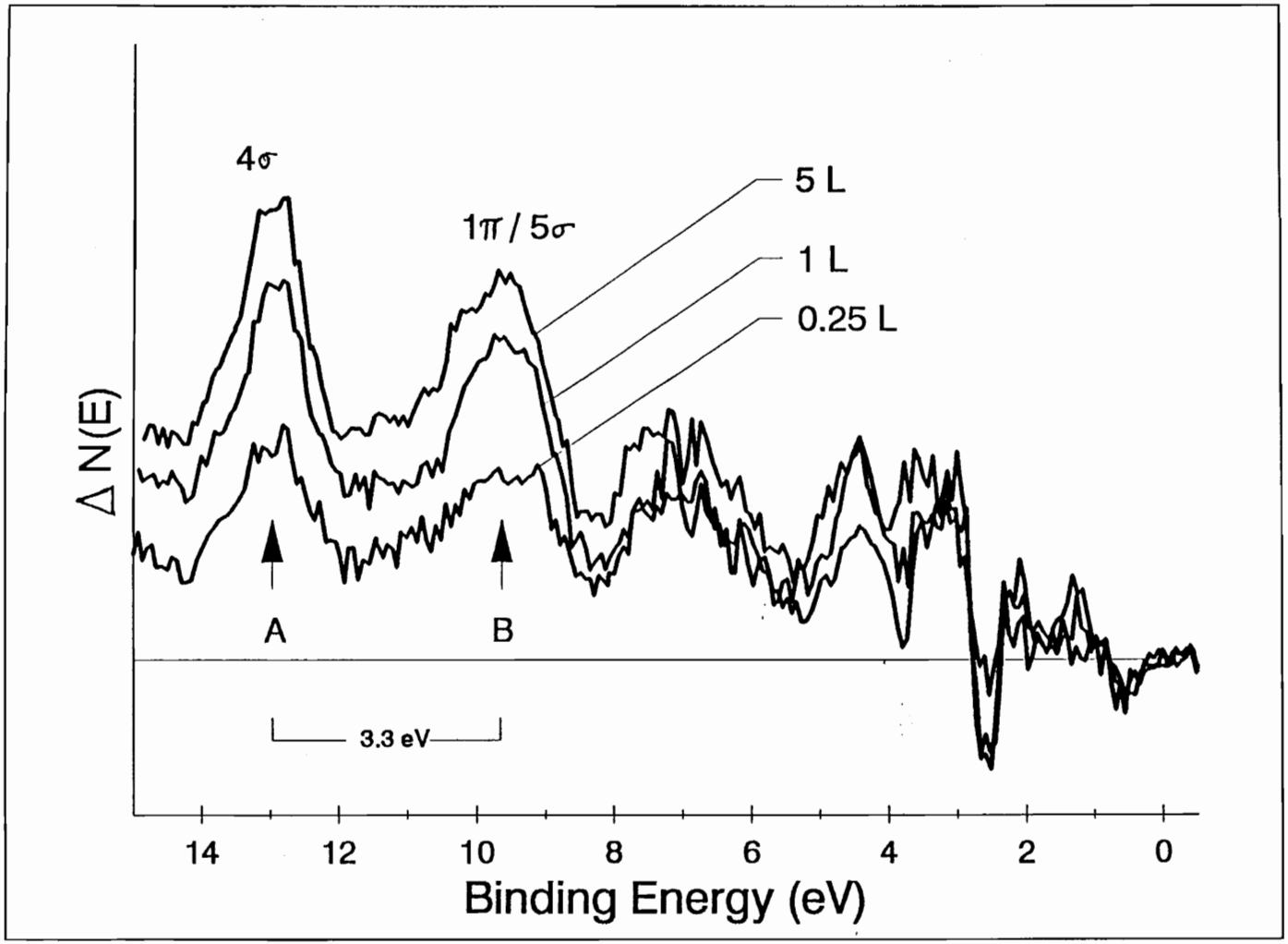

Figure 3.6 Difference curves associated with the He II UPS spectra (see figure 3.5) for CO adsorbed at 105 K on the nearly stoichiometric surface.

higher than 4.5 eV, two additional peaks, A and B, are observed at 9.6 and 12.9 eV. These features are consistent with previous studies of CO adsorption on other surfaces [45,46], and also with the gas-phase photoemission of CO [29,46], included in the inset of figure 3.5. The two CO-induced features, A and B, are clearly distinguished also in the difference spectra in figure 3.6. The two features at 9.6 and 12.9 eV have a separation of about 3.3 eV, similar to the 4σ-1π separation observed in gas-phase CO, transition metal carbonyls, and CO on Cu(100) and Ni(100) [45]. For CO on Cu(100) and Cu_2O(100), the 5σ orbital overlaps the 1π [48,45]. We interpret our spectra for adsorbed CO on Cu_2O(111) similarly to that of CO on Cu_2O(100) [45]: the 12.9 eV feature is derived from the CO 4σ orbital, and the 9.4 eV feature is due to an overlap of CO 1π and 5σ-derived orbitals. The decrease in the separation of the 4σ and 5σ levels upon CO adsorption and the similarity in the 4σ-1π splitting to gas-phase CO is characteristic of a CO molecule terminally bonded by the carbon atom. Previous studies of CO on Cu(100) put the 5σ level a few tenths of an eV *lower* binding energy than the 1π level using the polarization dependence of the two orbitals [48]. Lin *et al.* [46], using angular dependent He II UPS, showed that the CO 5σ orbital shifts to deeper binding energy, an observation consistent with studies of CO on ZnO [46]. We are unable to make such a distinction in our data because of the unpolarized UV source and the restricted detection geometries allowed by our rod-based sample manipulator.

Besides the CO-derived features (peaks A and B) in the difference curves, a number of other features are evident in the 0 to 8 eV range.

Because of the importance of d-band back-donation in the antibonding CO $2\pi^*$ orbitals in the Blyholder model of CO adsorption [49], we have paid particular attention to the features near 4 eV to determine if they result from a stabilization of the Cu d bands by a bonding interaction with the CO $2\pi^*$ level, as has been reported for Cu adatoms on ZnO single-crystal surfaces [50]. Examination of the difference curves demonstrate that these features are dependent on the normalization and alignment of the Cu d band necessary to obtain the difference spectra. Therefore, it is not possible to interpret these features near 4 eV as arising from the metal d band stabilization. However, examination of the unnormalized (He II UPS) spectra showed that, assuming a difference in elastic background, the two Cu_2O valence band features below 4 eV are found to experience the same attenuation from the CO overlayer to within a few percent relative to the background. Since the kinetic energies associated with the photoelectrons from these two sets of electronic states differ by only 2 eV, they should have similar mean free paths. The nearly identical attenuation demonstrates that the positive 4 eV feature obtained in the difference spectra may be the result of a simple increase in inelastic background. Similarly, no significant broadening or narrowing of the d-band emission is observed; the FWHM of the Cu d-band feature following CO adsorption is within 5 % of that of the clean surface, again suggesting a simple attenuation by the adlayer. Thus, all the features in the difference curves between 0 and 4 eV, positive and negative, may be explained by an increased inelastic background following CO adsorption. Also, small variations in the data manipulation (i.e., normalization and alignment)

necessary to obtain the difference spectra showed that it affected the intensity of the 7 eV feature. Therefore, it can not be assigned to the 5σ-derived orbital of CO, as may be first thought when comparing the gas-phase spectrum of CO and the UPS difference spectra.

A small successive shift of CO-induced peaks A and B to deeper binding energy is observed with increasing CO coverages. This shift is a general feature of CO adsorption and has been attributed to a change in relaxation associated with higher coverage [46].

He I UPS spectra were collected as well. Figure 3.7 shows the variation of the He I energy distribution curves for doses of 1 and 5 L at 120 K. As observed on He II UPS spectra, the features between 0 and 8 eV are derived from the valence band structure of the $Cu_2O(111)$ surface. Features in the photoemission spectrum from 5-8 eV are primarily O 2p (oxide) bands, while the density of states in the 1-4 eV range is primarily derived from Cu 3d bands [27,28]. The low binding feature below 1 eV near the VBM is associated with primarily Cu sp and O p interactions [27]. One CO-induced feature may be observed near 9.6 eV while the second one is seen near 12.9 eV in the inelastic tail.

The EDCs show that the two features observed in the 4 to 8 eV range are attenuated by CO adsorption, and that the attenuation is not uniform. For the clean $Cu_2O(111)$ surface, two features are observed in this region at 5.9 and 7.3 eV with the *higher* binding energy feature (7.3 eV) exhibiting the greater intensity. CO adsorption while reducing the intensity of both peaks, reverses the relative intensities so the *lower* binding energy feature (5.9 eV) exhibits the greater absolute intensity.

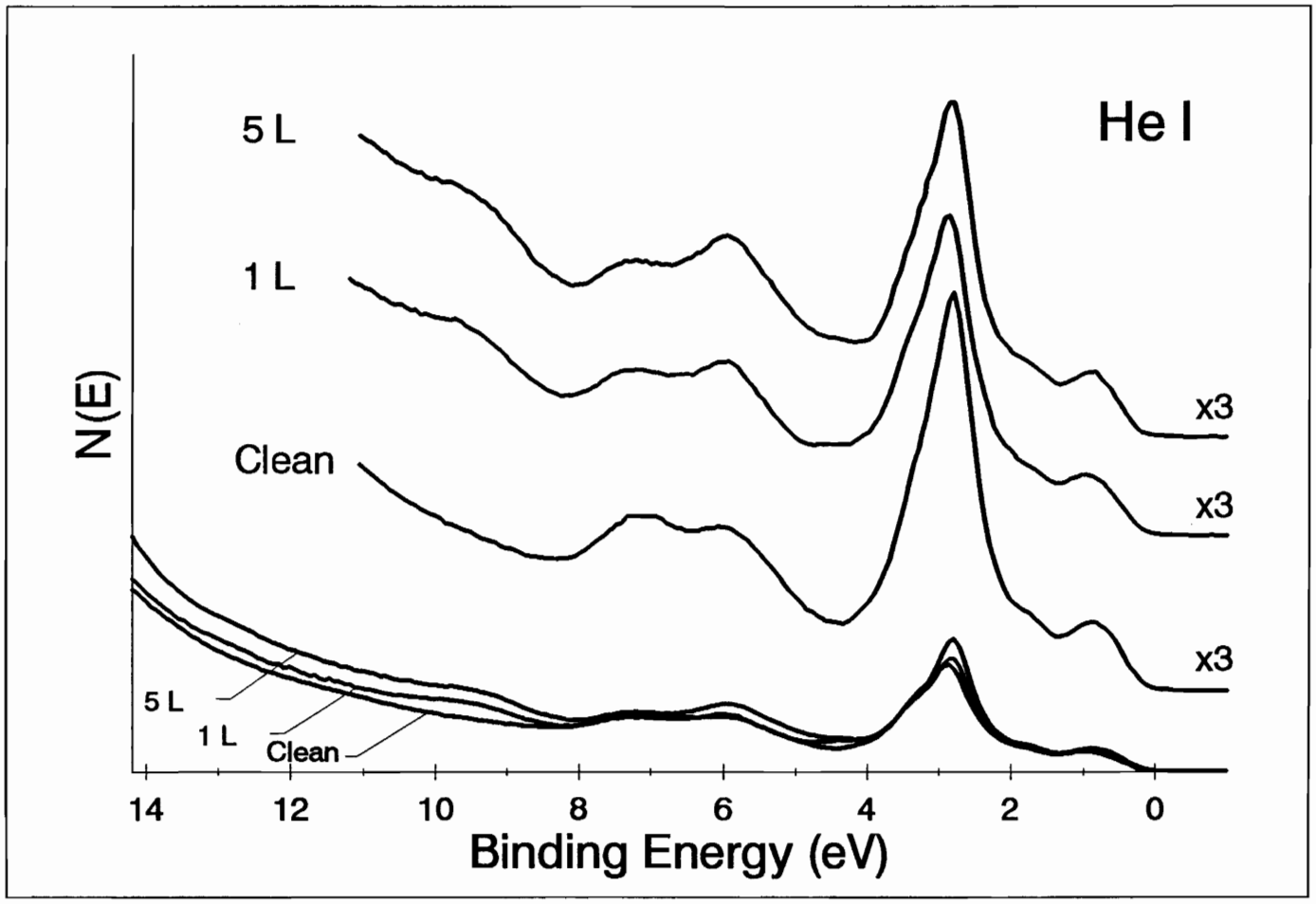

Figure 3.7 He I UPS spectra for CO adsorbed at 105 K on the nearly stoichiometric $Cu_2O(111)$ surface. All curves are aligned to the VBM at zero.

The attenuation of the 7.3 eV feature relative to background is *greater* for a given dose than that of the lower binding energy features in the range of 0 to 4 eV. In contrast, the 5.9 eV feature exhibits *less* attenuation than the lower binding energy (higher kinetic energy) features suggesting a net increase (excluding simple attenuation) in the density states at 5.9 eV.

One important difference was observed between the He I and He II UPS spectra for adsorbed CO. The nonuniform attenuation of the 5.9 eV and 7.3 eV features observed with He I was *not* observed with He II radiation; only a uniform attenuation was observed in He II UPS. Since the largest contribution to the photoemission features in the He II energy range is due to substrate O 2p bands [27,28], the photoionization cross section, $\sigma(h\nu)$, of the electronic states responsible for the relative increase in the 5.9 eV feature with He I must decrease more rapidly than the cross section for O 2p states with the change from He I to He II radiation. For O 2p, σ(He I)/σ(He II) = 10.67 Mb/6.816 Mb [47]. Some insight into the cause of the CO-induced change in relative intensities of the 5.9 and 7.3 eV features in He I but not He II is found by examining Robertson's bulk band structure calculation for Cu_2O [27].

Robertson's report of tight-binding (TB) calculations of the bulk Cu_2O band structure reproduces the experimentally observed optical gap (2.2 eV), and provides a partial density of states with which to compare the photoemission results described above [27]. The two features in the 4 to 8 eV range typically associated with O 2p (oxide) states also contain significant Cu 4s, 4p, and 3d character in the bulk [27]. We note that the Cu 3d character in this binding energy range has been confirmed

experimentally by valence band XPS which is sensitive primarily to Cu 3d states because of the high photoionization cross section relative to O 2p at high photon energies [45]. Using the symmetry of the bands at Γ as representative of the zone-averaged values in the bulk, the TB calculations suggest a 7.3 eV with mixed character: 60% O 2p, 9% Cu 4s, and 31% Cu 3d [27]. The 5.9 eV feature is much more ionic in the bulk: 84% O 2p and 16% Cu 3d [27]. A comparison of cross sections for Cu-derived states shows an increase for both Cu 3d, σ(He I)/σ(He II) = 7.553 Mb/9.934 Mb , and Cu 4s, σ(He I)/σ(He II) = 0.036 Mb/0.041 Mb, on changing form He I to He II [47]. Hence, the relative increase in the 5.9 eV feature in the He I UPS is not due to a direct involvement of Cu 3d and Cu 4s bands in the chemisorption bond or the nonuniform attenuation would be greater with He II radiation. While photoionization cross sections are not available for the normally unoccupied Cu 4p states of atomic Cu, a comparison with the 4p cross sections for higher-Z elements (Ge, As, Se) [47] suggests that nearly an order of magnitude *decrease* may be expected for Cu 4p-derived states with a change from He I to He II radiation. The relative increase in the 5.9 eV feature observed in He I but not He II can be attributed to a direct interaction of adsorbed CO with the Cu 4p-derived states of coordinately unsaturated Cu^+ cations. Hence, the character of the bulk bands at Γ and the variations in photoionization cross section of the metal electronic states suggest a direct Cu 4p component in what may reasonably be described as a CO 5σ donor bond to a hybridized Cu 4sp orbital. It is also noted that the photoionization cross section for Cu 4s states is so low that it is expected to contribute little (and hence cause no

significant change on rehybridization) to the photoemission intensity in either He I or He II UPS.

Figure 3.8 shows the variations in surface dipole, $\Delta\chi$, as a function of dose for water exposure for the nearly stoichiometric surface. While charging effects at low temperature make it impossible to accurately determine the changes in work function ($\Delta\Phi$) or band bending with UPS, it is still possible to determine changes in the surface dipole by aligning the Cu_2O valence band features at low binding energies (i.e. those in the 0 to 4.5 eV range which show no significant change in shape) and measuring the variation in the relative position of the vacuum level cutoffs. This procedure accounts for all shifts due to charging and band bending so that the variation in the position of the vacuum level cutoff contains only the changes in surface dipole, $\Delta\chi$.

As shown in figure 3.8, the surface dipole decreases monotonically with CO exposure. $\Delta\chi$ decreases most dramatically for doses below 0.5 L where the sticking coefficient is highest, then decreases slowly with increasing dose for a total change of about 0.6 eV, similar in magnitude to the decrease observed for CO on $Cu_2O(100)$ [45]. As with CO on $Cu_2O(100)$ and on ZnO($10\underline{1}0$) [46], the decrease in surface dipole implies polarization of the molecule by charge transfer to the surface to give a partial positive charge on the carbon atom [45,50]. These observations are consistent with a strong σ-bonding interaction with the surface and a weak π-backbonding contribution [45].

The change of surface dipole for the oxygen-deficient surface at 125 K is also shown in figure 3.8. Within the error-bars (evaluated to be

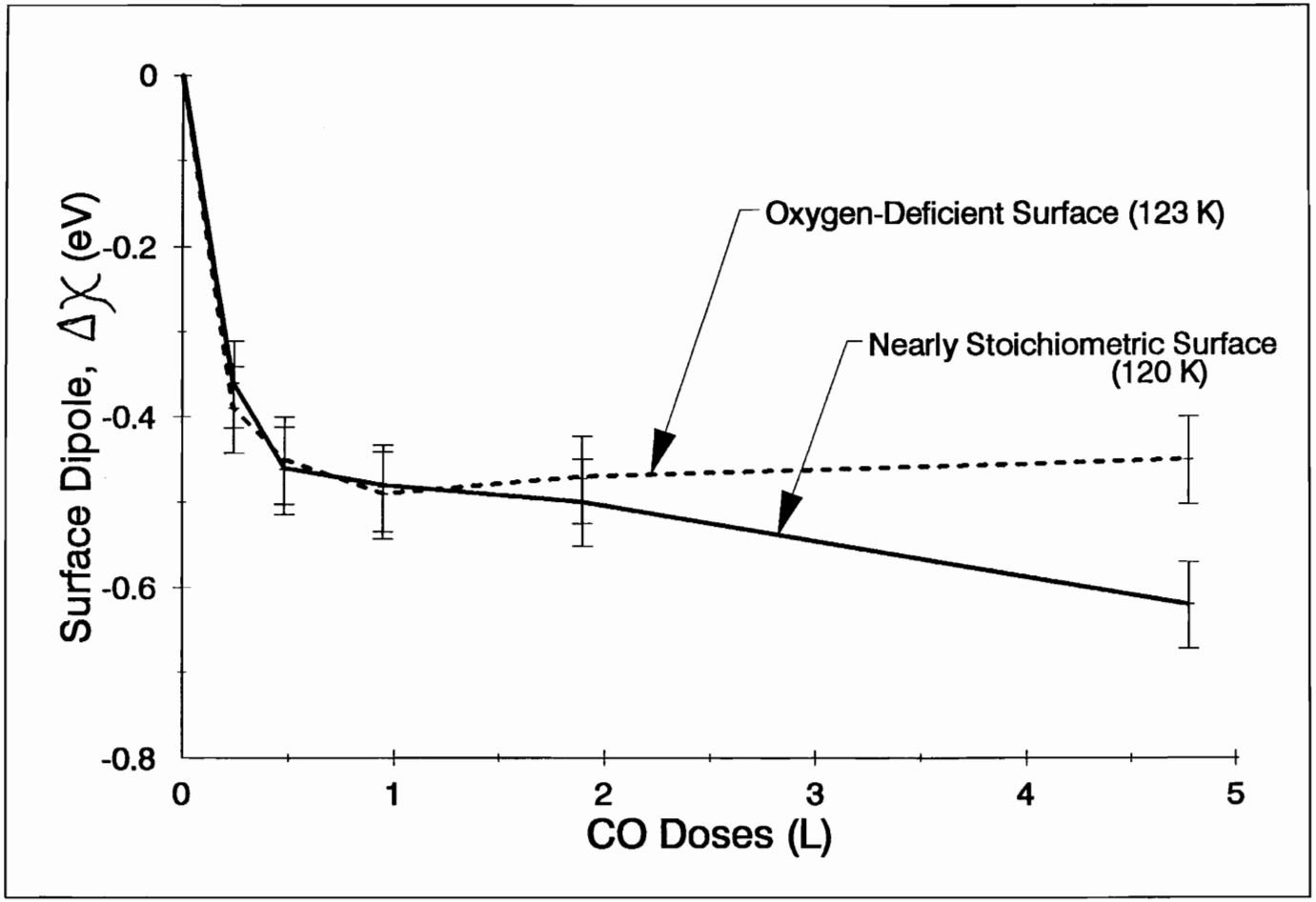

Figure 3.8 Variation in the surface dipole for the nearly stoichiometric (solid line) and the oxygen-deficient $Cu_2O(111)$ surface

about ± 0.05 eV from the data manipulation, i.e. normalization, alignment of the Cu 3d band emission as well as alignment of the vacuum level cutoff), the variation of surface dipole with CO doses for the oxygen-deficient surface shows the same trend to that observed on the nearly stoichiometric surface over most of the range of doses investigated.

UPS (He II) following CO adsorption at 105 K on the oxygen-deficient $Cu_2O(111)$ surface was similar to that of figure 3.5, showing that on such a defective surface, CO adsorption is molecular as well.

Thus, UPS measurements do not allow us to distinguish any major difference upon CO adsorption for the nearly stoichiometric and the oxygen-deficient $Cu_2O(111)$ surface.

3.2.3 X-Ray Photoelectron Spectroscopy (XPS)

Figure 3.9 presents X-Ray photoemission spectroscopy (XPS) data on the C 1s (CO 2σ) core level for the CO-adsorbed $Cu_2O(111)$ surface. The spectrum was referenced according to the accepted position of the Cu $2p_{3/5}$ photoemission peak in Cu_2O (B.E. = 932.4 eV). The C 1s photoemission spectrum exhibit a strong satellite structure, as observed previously by Solomon and co-workers for a CO-adsorbed CuCl(111) surface [46]. The main peak is observed near 288 eV, as referenced to Cu $2p_{3/5}$ peak, and is followed by a satellite that is $\approx$ 5.5 eV to deeper binding energy with an intensity (determined from the integrated areas of

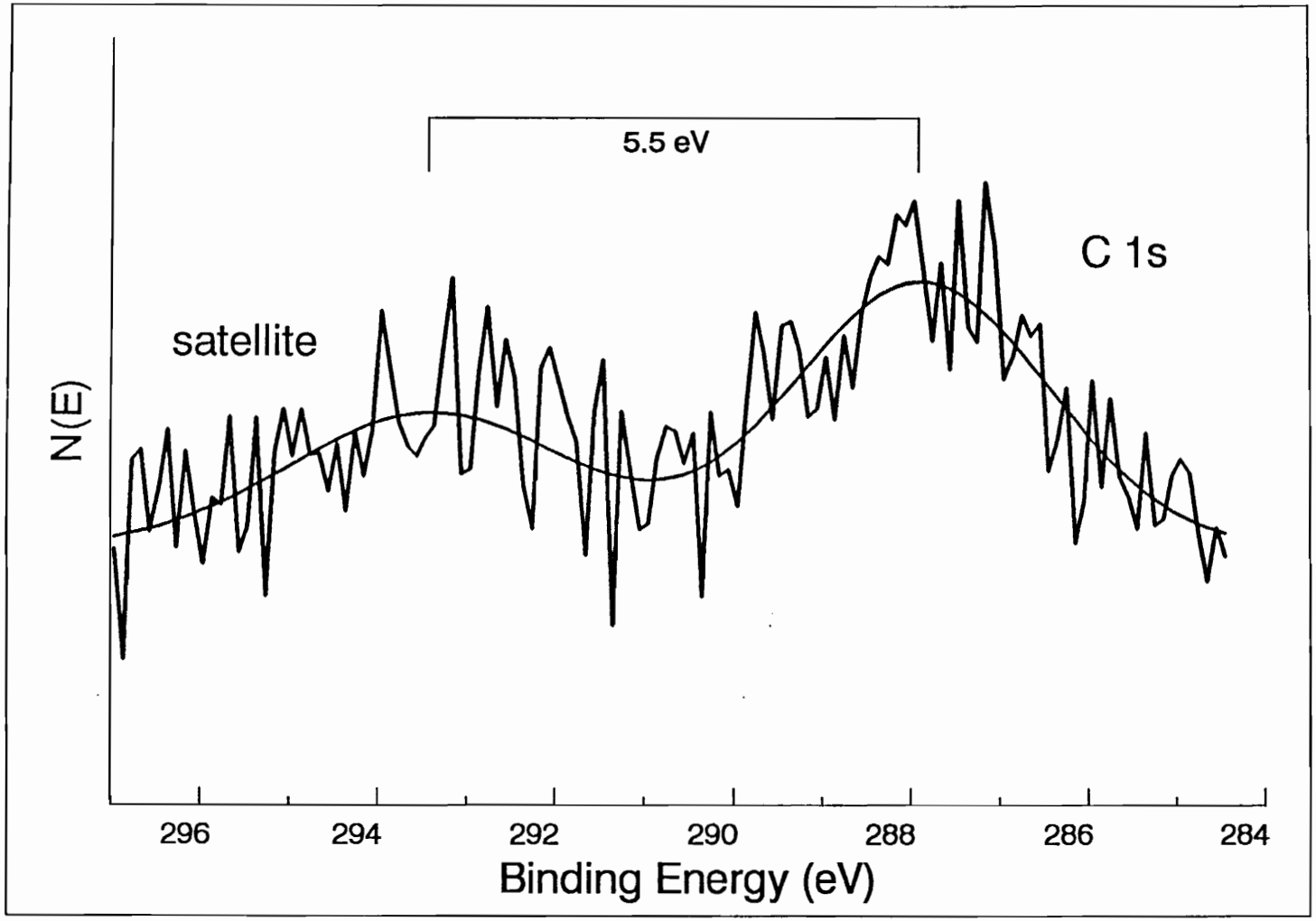

Figure 3.9 XPS C 1s spectrum for 60 L of CO on the nearly stoichiometric $Cu_2O(111)$ surface at 105 K.

the fitted curves in figure 3.9) of 50 % relative to that of the main peak.

The main peak (observed at lower binding energy) is often referred to as a shake-down peak [46]: the charge transfer from the metal d band into the unoccupied CO $2\pi^*$ level creates a core level hole, which results in relaxation. As a consequence, the CO ($2\pi^*$) level stabilizes to lower energy than the metal d band. The satellite peak, referenced as the satellite structure of the CO core levels, observed at deeper binding energy than that of the main peak, has been reported for many transition metal surfaces as well as for the CuCl(111) surface by Solomon and co-workers [46]. It is generally accepted as evidence for the presence of π-backbonding in the CO bond to the surface cations [46]. The relative intensity of the satellite peak ($Area_{(sat)}/Area_{(main)}$) is related to the extent of π-backbonding [46]. Therefore, it has been shown that, as the extent of π-backbonding decreases, the satellite peak becomes more intense. For CO on Ni(100), known for strong π-backbonding, the satellite peak represents about 35 % of the C 1s main peak. In contrast, for CO adsorbed on Ag(110), which is an example of weak π-backbonding, the intensity of the satellite peak is greater than that of the main peak. According to these two examples, π-backbonding for CO binding on $Cu_2O(111)$ appears to be of intermediate strength, as shown by the ratio, $Area_{(sat)}/Area_{(main)}$, equal to 50 $\pm$ 5 %.

The XPS results for the oxygen-deficient surface show the satellite peak as well, that is about 5.6 eV to deeper binding energy than the main peak (C 1s), observed near 287.5 eV, referenced as described above. Hence, the results on the oxygen-deficient surface are similar to that

observed on the nearly stoichiometric $Cu_2O(111)$ surface for CO adsorption. The presence of threefold sites of singly-coordinate Cu^+ cations at oxygen vacancies do not appear to greatly affect CO adsorption on the $Cu_2O(111)$ surface.

3.3 Discussion

The TDS results can be explained as follows. A higher temperature desorption state, 360 K, for CO on $Cu_2O(111)$ was observed in comparison to a maximum of 270 K for CO adsorption on $Cu_2O(100)$ [45]. The activation energy for desorption of CO from that highest-temperature binding state on the $Cu_2O(111)$ surface (Tp = 360 K in TDS) is 22 kcal/mol. The constant sticking coefficient for doses up to 0.5 and 0.25 L, respectively for the nearly stoichiometric and the oxygen-deficient surfaces, suggests a precursor state and non-activated adsorption as seen on $Cu_2O(100)$ and Cu(110) [45]. Hence, the measured activation energy for desorption is equivalent to ΔH_a. Most of the studies of CO adsorption on other surfaces give values for ΔH_a below 15 kcal/mol [45] and two values are reported in the 15-17 kcal/mol for metallic copper surfaces [45]. However, similar heats of adsorption were previously reported for CO binding on CuCl(111) (ΔH_a = 23 ± 2 kcal/mol) [46], for CO on Cu_2O powders (ΔH_a = 20.8 kcal/mol), as well as for CO on Cu/ZnO catalysts

(18 - 21 ± 2 kcal/mol, experimentally; 22.4 kcal/mol, theoretically).

Different types of chemisorption are observed on a variety of transition metal surfaces [46]. It can be dissociative, as normally observed for transition metals to the left of the periodic table with heats of adsorption as high as 60 - 90 kcal/mol: π-backbonding is very strong, leading to C-O bond rupture. Chemisorption can be strong and non dissociative, as observed for group VIII transition metals at or below room temperature with heats of adsorption ranging from 28 kcal/mol on Ni to 45 kcal/mol on Pd. CO adsorption of this type results in an increase in the work function and a decrease in the CO stretching frequency: π-backbonding dominates the CO bonding to the surface. But, chemisorption can also be weak and non dissociative as observed for group IB metals with heats of adsorption under 15 kcal/mol. Although π-backbonding still appears to dominate in the Cu(0)-CO bond (evidenced by a small decreased in CO stretching frequency [46]), CO-covered Cu(0) shows a small decrease in the surface work function and CO adsorbed on Ag and Au surfaces both have higher stretching frequencies [46]. On moving from left to right in the periodic table, the ability of a transition metal to donate charge in the CO $2\pi^*$ orbital decreases with higher effective nuclear charge [46].

It has been suggested that the increased heat of adsorption for CO bound at Cu^+ cations in a ZnO matrix relative to that of Zn^{2+} cations is due to a backdonation of charge from Cu 3d states (which lie at higher binding energy than the Zn 3d states) to the CO $2\pi^*$ orbitals. Indeed, the increased strength of σ-bonding and the presence of π-backbonding leads

to a stronger metal-CO bond, and therefore an increase of ΔH_a. In experimental studies of CO interactions with Cu metal and Cu^+ overlayers on ZnO single-crystal surfaces, Didziulis *et al.* [50] suggest that there is both a stronger π-backbonding interaction and a stronger σ-donor interaction (relative to ZnO) between CO and both different forms of supported copper. Their evidence for the increased CO σ-donor interaction was a stabilization of the CO 5σ level relative to that observed for CO on ZnO [50]. For the increase in π-backbonding, CO-induced variation in valence band photoemission features were attributed to a stabilization (i.e., increase in binding energy) of Cu 3d states for both metallic Cu and Cu^+ overlayers on ZnO single crystal surface [50]. Similarities in these changes of the valence band features for Cu^0 and Cu^+ were taken as an indication of similar extents of π-backbonding on the two ZnO-supported copper species.

The UPS data collected for CO adsorption on $Cu_2O(111)$ is similar to that of CO on $Cu_2O(100)$. Comparison of the photoemission spectra for CO on $Cu_2O(111)$ (figure 3.7) and Cu(100) [45] also suggests similarities in the bonding between Cu^+ and Cu^0. While we are unable to resolve the details of the ordering of the CO 1π and 5σ orbitals which might indicate greater 5σ stabilization for greater CO σ-donor character, the similarity in the 4σ-$1\pi/5\sigma$ separation suggests that the σ-bonding components do not differ greatly between Cu^+ and Cu^0 on extended surfaces. However, the UPS data shows no clear evidence of significant d-band stabilization. For $Cu_2O(100)$ and Cu(100), there are some apparent differences in the interaction of CO with Cu^0 and Cu^+. For metallic copper surfaces the

work function goes through a minimum usually below half a monolayer coverage [45]. Cu(100) exhibits the smallest change in work function of about 0.2 eV [45], while the Cu(111) surface shows the largest reported work function decrease of 0.45 eV [45]. It has been suggested that CO on Cu is bound primarily via a σ-bond donating charge to the metal with a small π-backbonding contribution to the CO $2\pi^*$ orbital. The modest work function change is believed to be due to the π-backbonding contribution which reduced the net charge transfer to the metal. For $Cu_2O(100)$, a larger change in surface dipole, $\Delta\chi$, is observed in comparison to the $\Delta\Phi$ observed on the metal surfaces (0.7 eV for a 5 L dose and 0.5 eV for a 0.5 L dose on $Cu_2O(100)$). These higher values, particularly in the low-dose range, demonstrate a higher *net* charge transfer to the surface which polarizes the CO molecules (i.e., CO exhibits more *net* donor character to Cu^+ than Cu^0 on extended surfaces). On the nearly stoichiometric $Cu_2O(111)$ surface, $\Delta\chi$ decreases to about 0.6 eV for a 5L dose of CO and $\approx$ 0.46 eV for a 0.5 L dose of CO. These values for the dipole changes on the $Cu_2O(111)$ surface are lower than those obtained for $Cu_2O(100)$, and may be due to increased π-backbonding contribution on $Cu_2O(111)$ compared to $Cu_2O(100)$. However, these differences in $\Delta\chi$ are small, and nearly within the error range of the measurements. Cox and Schulz, without ruling out a contribution of π-backbonding in CO bonding to the (100) surface [45], do not report any XPS data which would give an indication of a π-backbonding contribution based on the presence of a C 1s satellite peak. Assuming that π-backbonding is larger for CO bound on $Cu_2O(111)$ than that on $Cu_2O(100)$ (if any), it would cause a net

increase in the surface dipole, resulting in smaller overall surface dipole changes for CO on the (111) surface than those for CO on the (100) surface as observed experimentally. Further XPS studies of CO on the (100) surface are needed to determine whether or not the observed variations in $\Delta\chi$ as well as in the heats of adsorption are due purely to π-backbonding interactions.

The net increase in ΔH_a and CO donor character to Cu^+ compared to Cu^0 can be considered in terms of changes in the σ-bonding and π-backbonding contributions to the chemisorption bond. For a constant σ-bonding contribution, a decrease in π-backbonding would lead to increased polarization (i.e., decrease in $\Delta\chi$ relative to that observed for CO on metallic copper) as observed experimentally, but would also be expected to decrease ΔH_a, in contrast to the experimentally observed increase. Conversely, while an increase in π-backbonding could account for an increase in ΔH_a, it does not account for the decrease in $\Delta\chi$ relative to metallic copper. Clearly then, relative changes in the extent of π-backbonding alone can not account for the experimental observations.

In contrast, an increase in the σ-bonding component alone could qualitatively account for all the experimental differences between CO adsorption on Cu^+ at the $Cu_2O(100)$ surfaces and Cu^0 on extended metallic surfaces. An increase in the CO σ-donor contribution should increase both the heat of adsorption and lead to increased polarization of CO with a concomitant decrease in $\Delta\chi$. Both of these effects are observed experimentally. The σ-bonding component is also consistent with the available vibrational spectroscopic data for $CO\text{-}Cu^+$, $CO\text{-}Cu^0$, and

CO-Zn^{2+} [45]. When σ-bonding is the most significant contribution, like for CO on ZnO, the C-O bond strengthens: the stretching frequency increases. For CO bonding to Cu^{+} cations on Cu/ZnO, the stretching frequency is higher compared to that of CO on metallic copper. CO is chemisorbed primarily by σ-bonding on metallic Cu surfaces, with some small π-backbonding contribution [45]. The backdonation of charge into the antibonding CO $2\pi^{*}$ orbital weakens the C-O bond as evidenced by a decrease in the CO stretching frequency. The increased stretching frequency for CO bonding to Cu^{+} cations on Cu/ZnO relative to that of CO bonding to metallic copper is qualitatively consistent with an increased σ-bonding component, similar to the σ-bonding-induced increase in stretching frequently observed for CO on ZnO [45].

While this discussion points to an increase in the σ-bonding component of the CO bond for Cu^{+} relative to Cu^{0} on extended surfaces, π-backbonding from the Cu 3d bands to the CO $2\pi^{*}$ has been evidenced by the observation of a satellite peak below the C 1s peak in the XPS spectrum for 60 L of CO adsorbed on $Cu_2O(111)$. Thus, angle/ polarization-resolved UPS is required to provide additional information on whether or not an increased stabilization of the CO 5σ-derived orbital is observed relative to metallic copper.

On $Cu_2O(100)$, the increased heat of adsorption compared to that on metallic copper was assigned to an increased CO σ-donor function (or Cu^{+} acceptor function) relative to Cu^{0}. Therefore, for $Cu_2O(111)$, it can be explained by strong and dominant σ-bonding with some π-backbonding interactions, leading to an increased CO-surface bond strength as

evidenced by the high heat of adsorption. The dominant σ-bonding character is evidenced by the decreasing surface dipole and by the observation of direct interaction of adsorbed CO with the Cu 4p-derived states of coordinately unsaturated Cu^+ cations. The net increase in charge transfer to the cation results in a more polarized CO molecule on Cu^+. In an attempt to understand the increased selectivity for methanol synthesis from CO and H_2 of Cu-containing ZnO catalysts relative to that of pure ZnO, Solomon and co-workers suggested that such a polarized CO molecule is then more susceptible to heterolytic attack by dissociative adsorbed H_2 [46].

Also, the observation that the heat of adsorption for CO on $Cu_2O(111)$ is significantly higher than that for CO adsorbed on $Cu_2O(100)$ suggests that the geometry of the adsorption sites increases the CO-surface cation bond strength. Cu_2O surfaces are peculiar because of the unusual linear O-Cu-O bonds in the bulk. From the observation of the local coordination on different crystallographic surfaces, the geometry of the adsorbing sites can be determined. The CO molecule is thought to bind to the surface unsaturated cations perpendicularly to the $Cu_2O(111)$ surface in order to satisfy the linear Cu^+ coordination of the bulk crystal. Solomon and co-workers suggested [46] that CO binds to the tetrahedral adsorption sites of the CuCl(111) surface similarly. Since CO ($2\pi^*$) orbitals are perpendicular to the CO molecular axis, they can interact with the copper 3d states, which are parallel to the surface. By contrast, the observation of the local geometry of a $Cu_2O(100)$ surface suggests that a highly-tilted molecule would be required to satisfy the symmetry of

the vacant coordination site on $Cu_2O(100)$. Steric hinderance could prevent such an alignment. The expected decrease in the CO $2\pi^*$/Cu d-band overlap would reduce the π-backbonding contribution to the chemisorption bond.

From the data collected with TDS, UPS and XPS, oxygen vacancies do not appear to influence CO adsorption on the $Cu_2O(111)$. However, as evidenced with the propene traces (TDS), the surface structure is thought to experience some changes upon CO adsorption. This effect is not yet understood.

3.4 Conclusions

Adsorption of CO on two types of $Cu_2O(111)$ surfaces was studied with TDS, UPS and XPS: molecular CO is the only product observed. Desorption of CO occurs at four temperatures in TDS: under 132 K, at 176 - 190 K, at 206 - 230 K. The high-temperature desorption state is associated with an activation energy of 22 kcal/mol. This high activation energy for desorption shows that molecular CO binds more strongly to the (111) copper oxide surface than to the (100) copper oxide surface: it is thought to be due to a strong σ-bonding with some π-backbonding interactions. Crystallographic orientation, hence the geometry of the adsorption sites, appear to have some influence the CO-surface cation

bond strength. CO adsorption on the oxygen-deficient surface was observed to produce changes in the surface structure. The presence of oxygen vacancies does not appear to affect CO chemisorption on $Cu_2O(111)$ surfaces.

CHAPTER 4

Summary and Recommendations for Future Work

The adsorption and dissociation of water molecules as well as the adsorption of carbon monoxide have been studied on $Cu_2O(111)$ stoichiometric and oxygen-deficient surfaces.

The adsorption of water resulted in water desorption from molecular species and recombination of dissociated species. The exact pathway for recombination of dissociated species is not known and can not be simply assigned to OH dispropornation as on many other surfaces. The desorbing species, the desorption kinetics and the extent of dissociation were similar on the nearly stoichiometric and the oxygen-deficient surfaces. Only $\approx$ 0.25 of a monolayer of water dissociates on $Cu_2O(111)$ regardless of surface condition. The local defect environment at oxygen vacancies does not play a significant role in the activity of the $Cu_2O(111)$ surface for the dissociation of water.

The study of CO adsorption on $Cu_2O(111)$ surfaces showed that CO adsorbs molecularly on these surfaces: no dissociation species are detected. The high heat of adsorption found (22 kcal/mol) relative to that on $Cu_2O(100)$ single-crystal surfaces and to that on metallic copper surfaces suggests that CO molecules bind strongly to the surface cations.

This is thought to be due to an increased σ-donor character in CO, with some π-backbonding interactions. Local defect environment around oxygen vacancies, as for water adsorption and dissociation, does not appear to play a significant role in the bonding of CO to the $Cu_2O(111)$ surface. Comparison of the present study of CO adsorption on $Cu_2O(111)$ surfaces with that of CO on a $Cu_2O(100)$ single-crystal surface showed that the geometry of adsorption sites, related to the crystallographic orientation, affect CO chemisorption on copper oxide surfaces.

Future work with CO adsorption on the $Cu_2O(100)$ surface may be interesting. For this (100) single-crystal surface, Cox and Schulz, even without ruling it out, did not observe any π-backbonding from the metal d band to the CO ($2\pi^*$) level [45]. Further XPS studies of CO adsorbed on $Cu_2O(100)$ would be useful to determine whether or not π-backbonding is present in the bond CO forms with the surface cations, and if the small differences observed in the surface dipole changes in between the (111) and the (100) surfaces are due to π-backbonding. This would help characterizing the role that crystallographic orientation, related to the adsorption sites geometry, plays in the adsorption of molecules on Cu_2O surfaces.

Repetition of theses studies using IRAS (Infrared Adsorption Spectroscopy) would be very helpful to determine the dissociation products formed from water dissociation, as well as to characterize the C-O bond with the surface cation.

At last, the use of angle-resolved UPS with polarized synchrotron

radiation would give further evidence of π-backbonding in the CO bond to the surface cations, along with σ-bonding characterization. Such studies would also allow to differentiate the real splitting of the 1π and 5σ orbitals, as well as the change transfer onto the carbon atom of the CO molecule upon adsorption, which could not be distinguished in our data because of the restriction of the experimental setup (unpolarized UV source, rod-based sample manipulator).

REFERENCES

[1] B. J. Mason, Clouds, Rain and Rainmaking, (2nd ed., Cambridge University Press, 1975); H. R. Pruppacher, J. D. Klett, Microphysics of clouds and precipitation, (Reidel, Dordrecht, 1978), pp 257-268.

[2] P. A. Shumskii, Principles of structural glaciology (Dover, New York, 1964).

[3] L. R. Faulkner, *J. Chem. Ed.* **60** (1983) 262; E. Gileadi, Interfacial electrochemistry (Addison-Wesley Reading, MA 1975).

[4] C. Leygraf, M. Henderwerk, and G. A. Somorjai, *J. Catalysis* **78** (1982) 31; J. E. Turner, *Chem. Phys. Letters* **105** (1984) 581.

[5] M. Van Thiel, E. D. Becker and G. C. Pimentel, *J. Chem. Phys.* **27** (1957) 486.

[6] K. H. Schulz and D. F. Cox, *Surface Science* **278** (1992) 9.

[7] G. B. Fisher and J. L. Gland, *Surface Science* **94** (1980) 446; G. B. Fisher and B. A. Sexton, *Phys. Rev. Lett.* **44** (1990) 683.

[8] C. Benndorf, C. Nöbl, M. Rusenberg, and F. Theime, *Surface Science* **111** (1981) 87.

[9] R. Stockbauer, D. M. Hanson, S. A. Flodström, and T. E. Madey, *Phys. Rev. B* **26** (1982) 1885.

[10] P. A. Thiel and T. E. Madey, *Surface Science Reports* **7** (1987).

[11] R. L. Kurtz, and V. E. Henrich, *Phys. Rev. B* **26** (1982) 6682.

[12] M. B. Hugenschmidt, L. Gamble and C. T. Campbell, *Surface Science* **309** (1994) 329.

[13] W. J. Lo, Y. W. Chung, and G. A. Somorjai, *Surface Science* **71** (1978) 199.

[14] D. Peng, and M. A. Barteau, *Surface Science* **233** (1990) 283.

[15] V. E. Henrich, *Reports on Progress in Physics* **48** (1985) 1481; V. E. Henrich, *Prog. Surf. Sci.* **9** (1979) 143.

[16] D. F. Cox and K. H. Schulz, *Surface Science* **256** (1991) 67.

[17] J. L. Loison, M. Robino and B. Schwab, *J. Cryst. Growth* **50** (1980) 816.

[18] K. H. Schulz and D. F. Cox, *Physical Review* B **43** (1991) 1610.

[19] P. W. Tasker, *J. Phys. C (Solid State Phys.)* **12** (1979) 4977.

[20] K. H. Schulz and D. F. Cox, *Surface Science* **262** (1992) 318.

[21] E. M. Stuve, S. W. Jorgensen, and R. J. Madix, *Surface Science* **146** (1984) 179.

[22] P. A. Thiel, F. M. Hoffmann and W. H. Weinberg, *J. Chem. Phys.* **75** (1981) 5556.

[23] J. J. Zinck and W. H. Weinberg, *J. Vac Sci. Technol.* **17** (1980) 188. R. I. Hedge and J. M. White, *Surface Science* **157** (1985) 17.

[24] M. Klaua and T. E. Madey, *Surface Science* **136** (1984) L42.

[25] V. A. Gercher and D. F. Cox, *Surface Science*, submitted.

[26] P. A. Redhead, *Vacuum* **12** (1962) 203.

[27] J. Robertson, *Physical Review B* **8** (1983) 3378.

[28] C. Benndorf, H. Caus, B. Egert, H. Seigel anf F. Theime, *J. Electron Spectrosc. Relat. Phenom.* **19** (1980) 77.

[29] D. W. Turner, C. Baker, A. D. Baker and C. R. Brundle, Molecular photoelectron spectroscopy, (Wiley-Interscience, New York, 1970) p. 113.

[30] J. A. Connor, M. Considine, I. H. Hillier, and D. Briggs, *J. Electron Spectrosc. Relat. Phenom.* **12** (1977) 143.

[31] J. M. McKay and V. E. Henrich, *Phys. Rev. B* **32** (1985) 6764.

[32] R. L. Kurtz, and V. E. Henrich, *Phys. Rev. B* **28** (1983) 6699.

[33] A. Many, Y. Goldstein, and N. B. Grover, Semiconductor surfaces (North Holland, Amsterdam 1971).

[34] R. H. Stulen and P. A. Thiel, *Surface Science* **157** (1985) 99.

[35] T. E. Madey and F. P. Netzer, *Surface Science* **117** (1982) 549; F. P. Netzer and T. E. Madey, *Phys. Rev. Lett.* **47** (1981) 292.

[36] K. Bange, D. E. Grider, T. E. Madey and J. K. Sass, *Surface Science*

136 (1984) 38.

[37] D. G. Aitken, P. A. Cox, R. G. Egdell, M. D. Hill and I. Sach, *Vacuum* **33** (1983) 753.

[38] P. A. Cox, R. G. Egdell and P. D. Waylor, *J. Electron Spectrosc. Relat. Phenom.* **29** (1983) 247.

[39] G. Zwicker and K. Jacobi, *Surface Science* **131** (1983) 179; R. Zhang, A. Ludviksson, and C. T. Campbell, *Surface Science* **289** (1993) 1.

[40] C. Benndorf, C. Nöbl, and T. E. Madey, *Surface Science* **138** (1984) 292.

[41] D. F. Cox and K. H. Schulz, *J. Vac. Sci. Technol. A* **8** (1990) 2599.

[42] K. H. Schulz and D. F. Cox, *J. Catal.* **143** (1993) 464.

[43] M. W. Abee and D. F. Cox, unpublished data.

[44] A.-C. Christiaen and D. F. Cox, manuscript in preparation.

[45] D. F. Cox and K. H. Schulz, *Surface Science* **249** (1991) 138; and references therein.

[46] J. Lin, P. Jones, J. Guckert, and E. I. Solomon, *J. Am. Chem. Soc.* **113** (1991) 8312; and references therein.

[47] J. J. Yeh and I. Lindau, *At. data Nucl. Data tables* **32** (1985) 1.

[48] C. L. Allyn, T. Gustafsson and E. W. Plummer, *Solid State Commun.* **24** (1977) 531.

[49] G. Blyholder, *J. Phys. Chem.* **68** (1964) 2772.

[50] S. V. Didziulis, K. D. Butcher, S. L. Cohen and E. I. Solomon, *J. Am. Chem. Soc.* **111** (1989) 7110.

[51] J. T. Yates Jr., *Surface Science* **299-300** (1994) 731.

[52] K. H. Schulz and D. F. Cox, *J. Phys. Chem.* **97** (1993) 3555; K. H. Schulz and D. F. Cox, *J. Phys. Chem.* **97** (1993) 97.

[53] J. L. Falconer and R. J. Madix, *Surface Science* **48** (1975) 393.

VITA

Anne-Claire Christiaen, daughter of Anne-Marie et Jean Christiaen, was born on December 15, 1970, in Versailles, France. She enrolled as a chemical engineer student at the Université de Technologie de Compiègne, France, in 1988. During the fifth and last year of her undergraduate education, she took part of the exchange program with Virginia Polytechnic Institute and State University in 1992 as a Master of Science student. In June 1993, she received her B.S. in Chemical Engineering from the Université de Technologie de Compiègne and pursued her M.S. in surface science at Virginia Tech. After completion of her Master of Science, she will start working on her Ph.D. degree in Chemical Engineering at VPI&SU.